ANTIFERROMAGNETIC RESONANCE IN HYDRATED COPPER CHLORIDE

J. UBBINK

ANTIFERROMAGNETIC RESONANCE IN HYDRATED COPPER CHLORIDE

PROEFSCHRIFT

TER VERKRIJGING VAN DE GRAAD VAN DOCTOR IN DE WIS- EN NATUURKUNDE AAN DE RIJKSUNIVERSITEIT TE LEIDEN, OP GEZAG VAN DE RECTOR MAGNIFICUS Dr J. J. L. DUYVENDAK, HOOGLERAAR IN DE FACULTEIT DER LETTEREN EN WIJSBEGEERTE, TEGEN DE BEDENKINGEN VAN DE FACULTEIT DER WIS- EN NATUURKUNDE TE VERDEDIGEN OP WOENSDAG 11 MAART 1953 TE 16 UUR

DOOR

JAN UBBINK

GEBOREN TE ZEVENHOVEN IN 1922

UITGEVERIJ „EXCELSIOR" — 'S-GRAVENHAGE

PROMOTOR: PROF. DR C.J. GORTER

VOORWOORD

Teneinde te voldoen aan de wens van de Faculteit der Wis- en Natuurkunde volgt hier een kort overzicht van mijn academische studie.

In September 1939 begon ik mijn studie in de Wis- en Natuurkunde te Leiden. Na November 1940, toen de colleges en practica gesloten werden, legde ik hier enige tentamens af. Toen in September 1941 ook hiertoe geen gelegenheid meer bestond in Leiden zette ik de studie aan de Vrije Universiteit te Amsterdam voort, waar ik in Maart 1943 het candidaatsexamen letter A aflegde. Sinds de bevrijding in 1945 werkte ik op het Kamerlingh Onnes laboratorium, terwijl ik mij voorbereidde voor het doctoraalexamen in de experimentele natuurkunde dat ik in December 1948 aflegde. Hiervoor volgde ik de colleges van Prof.Dr.H.A.Kramers, Prof.Dr. J.de Boer en Prof.Dr.J.Droste. In de jaren 1946 - 50 was ik in het genot van een B.P.M. studieprijs. Mijn werkzaamheden op het Kamerlingh Onnes laboratorium werden in 1947 voor drie maanden onderbroken, welke ik in Oxford besteedde om mij te orienteren op de microgolventechniek voor experimenteel physische doeleinden. Sinds 1947 heb ik, onder leiding van Prof.Dr.C.J.Gorter en in samenwerking met J.A.Poulis en later ook met H.J.Gerritsen de microgolventechniek toegepast eerst op het onderzoek van de paramagnetische resonantie in ijzeraluinen en later op dat van de antiferromagnetische resonantie in koperchloride.

CONTENTS

Introduction 9

Chapter I. Theory 11
A. Static antiferromagnetism 11
1. Introduction 11
2. Theory neglecting the anisotropy energy 13
3. Theories including the anisotropy energy 16
4. The anisotropy energy according to YOSIDA 17
5. Flop-over of spins, critical field 19
6. Theory of GORTER and HAANTJES 19
7. The solutions of equations (36) and (37) 22
8. The realised solutions in the coordinate planes of h-space 24
9. Comparison between the theories of YOSIDA and of GORTER and HAANTJES 26
10. Discussion. Other theories 27
B. Antiferromagnetic resonance 31
1. Introduction 31
1.1. One spin 31
1.2. More spins 33
1.3. Anisotropic g-tensor 34
1.4. The resonance condition in antiferromagnetism 35
2. The resonance condition derived by YOSIDA, applying to copper chloride 36
3. The resonance condition derived on the basis of the static solutions of GORTER and HAANTJES 37
3.1. Formulae in the coordinate planes 39
3.2. The resonance condition at zero frequency 39
3.3. The resonance fields parallel to the axes as functions of the frequency 41
3.4. Properties of the resonance surface on Ω and Γ 42
3.5. The resonance condition for increasing frequency 43
4. Discussion

Chapter II, Experimental equipment and method of measurement 47
1. Introduction 47
2. The experimental equipment 47
3. Oscillators 48
4. Resonant cavities 50
5. The 3 cm resonance cavity 51
6. The 7 cm resonance cavity 52

7. The transmission lines 53
8. Detectors 54
9. The measurement of frequency 55
10. Method of measuring the absorption 55
11. The copper chloride crystals 56
12. The orientation of the crystal with respect to the external field 57
13. The orientation of the high frequency field in the cavity 57

Chapter III. Experimental results 59
Introduction 59
A. The paramagnetic resonance measurements 60
B. The 3 cm antiferromagnetic resonance measurements 61
1. Introduction 61
2. Line positions 63
3. Shapes of the absorption curves 67
4. Intensities of the absorption 67
5. Remarks 70
C. The 7 cm antiferromagnetic resonance measurements 71

Chapter IV. Theoretical interpretation of the experimental results and discussion 75
1. The resonance curves in the coordinate planes at 3 cm wavelength 75
2. The resonance fields along the axes as functions of temperature at 3 cm wavelength 77
3. Discussion of the 7 cm results 82
4. Final remarks 83

Samenvatting 85

References 86

INTRODUCTION

Since the early work of THÉORIDÈS[1] and of WOLTJER and KAMERLINGH ONNES[2] who found that the magnetic properties at low temperatures had neither a paramagnetic nor a ferromagnetic character, many researches have been carried out on antiferromagnetic substances.

The basic picture underlying the description of antiferromagnetism is that the elementary magnets tend to be orientated alternately in opposite directions. This leads to a long range order of the magnetic moments which sets in at a critical temperature, the Néel temperature. In the molecular field theory of antiferromagnetism, Weiss molecular fields are introduced such that the molecular field acting on an ion is proportional but opposite to the average magnetization of its nearest neighbours. The foundations of this theory are mainly due to NÉEL.

The measurement of microwave magnetic resonance absorption, which found such a wide application in paramagnetism and to a lesser extent in ferromagnetism, might be expected to yield interesting data about antiferromagnetism. Theoretical considerations, however, suggested that for substances with Néel temperatures of the order of 100°K or higher, the magnetic fields at which resonance would occur would be too high to be experimentally realized. It was also recognized from the beginning that crystalline anisotropy would play an essential rôle. Thus, single crystals of substances with very low Néel temperatures would be the most favourable samples for the investigation of antiferromagnetic resonance. The measurements on powdered specimens of substances with relatively high Néel temperatures yielded only very weak resonance absorption below the Néel temperature [3,4].

When, therefore, it was found that copper chloride, $CuCl_2.2H_2O$, becomes antiferromagnetic below 4.3°K, it was reasonable to expect that single crystals of this substance would exhibit resonance in the microwave region at practicable fields. This expectation has been confirmed by the antiferromagnetic resonance absorption measurements on single copper chloride crystals which form the subject of this thesis *).

In Chapter I sec.A we give a survey of the molecular field theory of antiferromagnetism. In Sec.B we give a theoretical analysis of antiferromagnetic resonance, based on this theory, and a survey of the contributions of other authors in this field.

The experimental method used in this investigation is a simple transmission loss technique which, with the experimental equipment, is described in Chapter II.

The results of this investigation are given in Chapter III. The main results are the typical dependence of the fields at which resonance occurs on the orientation of these fields with respect to the crystal axes of the sample, and the dependence of these fields on temperature.

In Chapter IV a comparison is made between the experimental results and the theoretical predictions. It appears that the molecular field theory is able to describe the results satisfactorily in a qualitative way, but that some quantitative discrepancies remain. These are closely connected with discrepancies already existing between the molecular field theory of antiferromagnetism and the magnetic and caloric behaviour of copper chloride.

---

1. Ph. Théodoridès, J.de Phys.et le Rad.3(1922)1.
2. H.R.Woltjer, Commun.Kamerlingh Onnes Lab.,Leiden No.173b; Proc.Kon.Akad.Amsterdam 28(1925)536. H.R.Woltjer and H. Kamerlingh Onnes, Commun.No.173c; Proc.Kon.Akad.Amsterdam 28(1925)544.
3. Trounson, Bleil, Wangsness and Maxwell, Phys.Rev.79(1950)542.
4. Okamura, Torizuka, and Kojima, Phys.Rev.82(1951)285.

*) Some of this work has already been published in the following papers:
N.J.Poulis J.van den Handel, J.Ubbink, J.A.Poulis and C.J. Gorter, Phys.Rev.(2) 82(1951)552, and Proc.low Temp.Conf., Oxford (1951).
J.Ubbink, J.A.Poulis, H.J.Gerritsen and C.J.Gorter, Commun. Kamerlingh Onnes Lab., Leiden No.288d; Physica 18(1952)361.
J.Ubbink, Phys.Rev.(2) 86(1952)567; Commun.Suppl.No.105b; Physica 18(1952).

Chapter I

THEORY

A. Static antiferromagnetism

1. *Introduction*

When the interaction between certain neighbouring magnetic ions in a magnetic substance favours antiparallel alignment of the magnetic moments of these ions, an ordering of the moments may occur at low temperatures in such a way that no net magnetization of the substance originates from this order. Phenomena correlated with this ordering effect are summed up under the name „antiferromagnetism".

The simplest theoretical attack on antiferromagnetism is made in the so called molecular field theory. This theory is an extension of the Weiss molecular field theory in ferromagnetism. In its simplest form it divides the lattice of magnetic ions into two interlocking sublattices, and it assumes that the interaction between the magnetic ions may be represented by internal magnetic fields (molecular fields), the field acting on one sublattice being parallel but opposite and proportional to the magnetization of the other sublattice. The magnetization of a sublattice is obtained from the statistical distribution of the magnetic moments of this sublattice in the vector sum of the molecular field and the external field. The introduction of the molecular fields is often based on the assumption that the magnetic ions interact only with their nearest neighbours. The division into two sublattices is then made in such a way that all nearest neighbours of an ion in one sublattice belong to the other sublattice. The interaction between nearest neighbours is generally ascribed to an exchange effect.

The division of the ions into two systems with separate magnetizations corresponds to a certain degree of order. This order will be counteracted by thermal agitation, and the degree of order will decrease with increasing temperature. At a certain critical temperature the order may disappear. At higher temperatures then the division into two systems has lost its physical meaning. This critical temperature is in some respects similar to the Curie temperature of ferromagnetism, but GORTER and HAANTJES[1] propose to

give it a name of its own and to call it the Néel temperature T_N.

In the two sublattices molecular field theory we may divide the energy of the system into three parts:

1. The energy resulting from isotropic interaction between the ions of one sublattice and those of the other. By isotropic we mean that the energy does not depend on the orientations of the moments with respect to the crystal axes, but only on their relative orientations. It is generally supposed to originate from exchange interaction and the molecular fields are then sometimes called the „exchange fields". The existence of this energy tends to align the moments of one sublattice antiparallel to those of the other sublattice.

2. The magnetic energy of the magnetic moments in the external field, which tends to align the moments in the direction of that field.

3. The anisotropy energy. This energy may arise from anisotropic interaction between the ions as well as from interactions of the ions with non-magnetic parts of the crystal. It results in a tendency to orientate the moments along one or more preferred directions, directions of easy magnetization in the crystal.

A picture of the essential features of the behaviour of the magnetization vectors of the two sublattices may be obtained by a reasoning essentially due to NÉEL:

Due to the exchange energy the magnetizations will be orientated nearly antiparallel, as long as the magnetic energy and the anisotropy energy are small with respect to the exchange energy. When an external field is applied either parallel or perpendicular to the antiparallel magnetizations, the corresponding susceptibilities $\chi_\parallel$ and $\chi_\perp$ are different with $\chi_\perp > \chi_\parallel$ (cf. sec. 2). As, therefore, the magnetic energy $-\frac{1}{2}\chi H^2$ is, in absolute value, larger in the perpendicular than in the parallel case, the magnetizations tend to orientate themselves perpendicular to the external field. The fact that $\chi_\perp > \chi_\parallel$ is evident when the temperature equals zero: then both sublattices are saturated and only the directions, not the absolute values, of the total effective fields experienced by the two sublattices are relevant. These directions are not affected by the external field in the parallel case as long as the external field is smaller than the exchange field and $\chi_\parallel = 0$. But in the perpendicular case they are both rotated somewhat towards the direction of the external field and $\chi_\perp \neq 0$. When now the anisotropy energy is taken into account, the direction of alignment is found by balancing the tendency of the magnetizations to be orientated perpendicular to the applied field and the tendency to be orientated parallel to the preferred direction.

From these considerations the occurrence of a critical field

may be inferred. With zero external field the magnetizations are aligned along the preferred direction, antiparallel in the two sublattices. When, now, an increasing field is applied in the preferred direction, the magnetizations will flop over to the perpendicular direction when the applied field passes the critical value at which the magnetic energy at perpendicular orientation equals the anisotropy energy.

The molecular field theory of antiferromagnetism was originally proposed by NÉEL[2] in connection with his work on magnetic properties of metals. It has been further developed by BITTER[3], VAN VLECK[4], GARRETT[5], NAGAMIYA[6], YOSIDA[7,8] and GORTER and HAANTJES[1]. BITTER derived an expression for the parallel susceptibility which, together with one for the perpendicular susceptibility, was obtained more generally by VAN VLECK. In VAN VLECK's theory, reviewed in sec. 2, the anisotropy energy has not explicitly been accounted for. The theories of NAGAMIYA and YOSIDA, which do introduce the anisotropy energy explicitly, are reviewed in sec. 3-6. These theories calculate the magnetizations to an approximation which is valid when the two magnetization vectors do not deviate much from the antiparallel position, i.e. for external field values small with respect to the exchange fields. In sec. 7-9 we discuss the theory of GORTER and HAANTJES which is not confined to small external fields but which, on the other hand, is valid only at zero temperature.

2. *Theory neglecting the anisotropy energy* (VAN VLECK[4]).

We will indicate the spins of one sublattice with index i and those of the second with index j. The exchange interaction between two neighbouring spins i and j is equivalent to a potential energy

$$V_{ij} = -\tfrac{1}{2} J \, (1 + 4 \, \mathbf{S}_i \mathbf{S}_j). \qquad (1)$$

J is the exchange integral and negative in an antiferromagnetic substance. $\mathbf{S}_i$ and $\mathbf{S}_j$ are the angular momentum vectors of the spins i and j and are measured in multiples of the quantum unit $\hbar$. Apart from an additive constant the effective potential energy acting on spin i is then

$$V_i = -2 \, J \, \mathbf{S}_i \Sigma_j \mathbf{S}_j \qquad (2)$$

where the summation Σ_j is to be extended over the nearest neigh-

bours of spin i. In the molecular field approximation this becomes

$$V_i = -2 J z \mathbf{S}_i \overline{\mathbf{S}}_j \tag{3}$$

where z is the number of nearest neighbours. As the spins i have a magnetic moment $g\beta\mathbf{S}_i$ (β is the Bohr magneton, g the Landé factor), the exchange field for the spins i is

$$\mathbf{H}_E^i = 2Jz\overline{\mathbf{S}}_j/g\beta, \tag{4}$$

as this is the field in which the magnetic energy of the spin i equals (3). The total effective field for the spins i is

$$\mathbf{H}^i = \mathbf{H} + \mathbf{H}_E^i \tag{5}$$

where $\mathbf{H}$ is the external field. Applying Boltzmann statistics to the spins i, assuming the direction of quantization of these spins to be that of $\mathbf{H}^i$, we find an average vector of the spin vectors i directed along $\mathbf{H}^i$ with an absolute value

$$|\overline{\mathbf{S}}_i| = S B_s(y_i), \quad \text{so that} \quad \overline{\mathbf{S}}_i = (\mathbf{H}^i/H^i)\, S B_s(y_i), \tag{6}$$

and similarly

$$|\overline{\mathbf{S}}_j| = S B (y_j), \qquad \overline{\mathbf{S}}_j = (\mathbf{H}^j/H^j)\, S B_s(y_j).$$

where

$$y_i = H^i Sg\beta/kT$$
$$y_j = H^j Sg\beta/kT$$

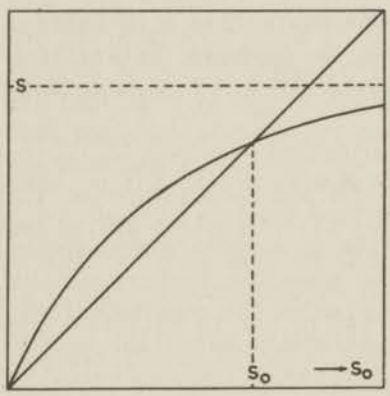

fig. 1.
S_o and $S B_s(y_o)$ as functions of S_o.

and B_S is the Brillouin function

$$B_S(y) =$$
$$= [(2S+1)/2S] \coth[(2S+1)y/2S] -$$
$$- (1/2S) \coth(y/2S). \tag{8}$$

When $S = \frac{1}{2}$, $B_S(y)$ reduces to $\tanh y$.

The average magnetic moments are found from

$$\mathbf{M}_i = g\beta\overline{\mathbf{S}}_i$$
$$\mathbf{M}_j = g\beta\overline{\mathbf{S}}_j$$

When we substitute (7), (5) and (4) into (6) and resolve the vectors in (6) into their components, the problem to find the average spin vectors as functions of temperature and external field is formulated in terms of six equations with six unknowns, the components of $\mathbf{S}_i$ and $\mathbf{S}_j$.

When $H = 0$ the average spin vectors will be equal and opposite on the two sublattices and their absolute value S_o can be found from

$$S_o = SB_S(y_o), \qquad y_o = 2zS|J|S_o/kT. \tag{10}$$

When we plot S_o and $SB_S(y_o)$ as functions of S_o we find the solution of (10) from the intersection of both curves. The Néel point is reached when S_o is reduced to zero, i.e. when (10) has a double root for $S_o = 0$. This leads to a Néel temperature

$$T = (2/3)|J|z\, k^{-1}\, S(S+1). \tag{11}$$

Solving the equations (6) with $H \neq 0$ and using (9) leads to the average magnetic moments in both sublattices. Giving **H** an infinitesimal value parallel or perpendicular to the direction of alignment we find with VAN VLECK that the corresponding initial susceptibilities are

$$\chi_{\parallel} = \delta M_{\parallel}/\delta H_{\parallel} = S^2 N g^2 \beta^2 B'_S(y_o)/k(T + 3T_N(S+1)^{-1} SB'_S(y_o)) \tag{12}$$

$$\chi_{\perp} = \delta M_{\perp}/\delta H_{\perp} = Ng^2\beta^2 S(S+1)/6kT_N. \tag{13}$$

N is the total number of spins. (The prime on B_S in (12) means differentiation with respect to its argument). Thus $\chi_{\perp}$ is independent of temperature and an analysis of $\chi_{\parallel}$ shows that it increases with increasing temperature from 0 for $T = 0$ up to $\chi_{\perp}$ for $T = T_N$.

VAN VLECK now assumes that in a powdered specimen the initial orientations are distributed at random and that thus the parallel and perpendicular case are represented in a ratio 1 : 2, so that the powder susceptibility will be

$$\chi = (1/3)(2\chi_{\perp} + \chi_{\parallel}). \tag{14}$$

The temperature dependence of the powder susceptibility which follows from (14) has been confirmed at least in a qualitative way. Yet we cannot be completely satisfied with VAN VLECK's theory for the following reason:

An analysis of the mathematical problem of finding $\overline{\mathbf{S}}_i$ and $\overline{\mathbf{S}}_j$

as functions of **H** from (6) shows that the only possible solutions, apart from those for which $\overline{\mathbf{S}}_i$ or $\overline{\mathbf{S}}_j$ or both equal zero, are solutions in which the vector $\overline{\mathbf{S}}_i - \overline{\mathbf{S}}_j$ (which is the direction of alignment for $H = 0$) is either parallel or perpendicular to **H**. Thus an oblique orientation is not possible. Moreover, as the perpendicular orientation has the lowest free energy, only this orientation would occur and the powder susceptibility would be $\chi_\perp$ and independent of temperature, in contrast with experiment. To overcome these difficulties it is necessary to introduce the anisotropy energy explicitly in one form or another.

3. *Theories including the anisotropy energy*

A theory including the anisotropy energy has been given by NAGAMIYA[6]. He assumes one or more axes of easy magnetization in the crystal and an anisotropy energy rotationally symmetric about these axes when the mean spin directions do not deviate much from the preferred directions. His calculations are confined to small deviations of the mean spin directions from the preferred directions. Therefore, his theory cannot describe the flop-over of the spins. The expressions derived for $\chi_\parallel$ and $\chi_\perp$ are in agreement with those of VAN VLECK, and the procedure of taking the powder susceptibility equal to $(1/3)(2\chi_\perp+\chi_\parallel)$ is justified. NAGAMIYA also derives a term of higher degree than the first in H in the net magnetization which results in a term with H^2 in the susceptibility. The resulting dependence of the susceptibility of field-strength should make it possible to determine the anisotropy constant. This of course will have sense only in the case where this dependence is detectable for fields so small that deviations of the mean spin directions from the preferred directions will remain small. We will not go into details of this theory as it does not include the flop-over of the spins, which is an essential feature in antiferromagnetism.

Detailed theories have been given by YOSIDA[7,8] in two papers, one specially adapted to the case of manganese fluoride MnF_2, the other to the case of copper chloride, $CuCl_2.2H_2O$, both including the flop-over effect. YOSIDA gives a detailed description of the anisotropy energy which we will review in the next section. In the case of copper chloride YOSIDA treats the complications of the anisotropy of the Landé factor due to the fact that there are two cristallographically different Cu^{2+}-ions per unit cell of the crystals of copper chloride. As YOSIDA, however, assumes the Landé factor to be isotropic in his discussion of the flop-over effect (cf.sec.5) and of the antiferromagnetic resonance[22], which

is our main interest, we will leave these complications out of consideration.

4. *The anisotropy energy according to YOSIDA*

The anisotropy energy of the antiferromagnetic substance may be considered to arise from the anisotropy of the electric crystalline field at the position of the magnetic ion and from such an anisotropic coupling between two spins as dipole-dipole interaction or anisotropic exchange interaction. The former part is expressible as a function of one spin variable, while the latter contains the spin variables of two magnetic ions.

The first type of anisotropy is treated in the first paper by YOSIDA[7] and applied especially to the case of manganese fluoride. The Mn^{2+}-ion has no orbital angular momentum in its free state (^6S). Its sixfold spin degeneration is removed only by higher order perturbation, through its excited states, of the crystalline electric field combined with spin-orbit interaction. From symmetry considerations YOSIDA makes it plausible that in the anisotropy part of the Hamilton an for the Mn^{2+}-ions a term $-DS_z^2$ will play the dominant rôle, and for reasons of simplicity only this term is adopted. Here S_z is the component of the spin angular momentum along the c-axis of the crystal.

The macroscopic anisotropy energy now may be considered to be the statistical average of the microscopic energy $-DS_z^2$. Assuming the average direction of the spins to have an angle φ with the z-axis, and each spin to be quantized along this direction, YOSIDA finds for the macroscopic energy, apart from an additive constant

$$f_{an.} = D' \sin^2\varphi \tag{15}$$

where
$$D' = D\,S^2[(S+1)/S - 3B_S(y_o)\,(1/2S)\coth(y_o/2S)] \tag{16}$$

and y_o has the same meaning as in (10).

When $S>\frac{1}{2}$ the macroscopic anisotropy energy constant D' decreases with increasing temperature and becomes zero for $T = T_N$. This corresponds to the fact that at the Néelpoint the spins are orientated at random and so there cannot be any dependence upon the orientation of the macroscopic energy. If $S = \frac{1}{2}$, however, the expression (16) vanishes identically. Thus, if we extrapolate these considerations to the case of copper chloride, we may conclude that this type of anisotropy does not play an important rôle in this case. Therefore we will consider the second type,

which results from anisotropic coupling between the spins, and which is treated in YOSIDA's second paper[8].

VAN VLECK[9] gives the general expression for the interaction energy between two spins of spin quantum number ½. Assuming that this energy is invariant against rotation about the line joining the spins, YOSIDA shows that this energy consists of an isotropic coupling of the exchange type, which depends only on the angle between the spin vectors, and of an interaction of the dipole-dipole type which also depends on the angles between the line joining the spins and the spin vectors. Assuming further:

1) the interaction exists only between certain (nearest) neighbours;
2) the molecular field hypothesis, i.e. the average over those neighbours is identified with the average over the whole corresponding sublattice,

it may be shown that the orientation-dependent part of the potential energy, due to interaction, acting on one individual spin $\mathbf{S}_i$ is:

$$V_i = (2|J|z+C_x)\bar{S}_{jx}S_{ix}+(2|J|z+C_y)\bar{S}_{jy}S_{iy}+(2|J|z+C_z)\bar{S}_{jz}S_{iz}. \quad (17)$$

An analogous expression holds for the potential energy V_j acting on a spin $\mathbf{S}_j$.

The macroscopic anisotropy energy is found by calculating the free energy of the system for a certain average direction of the spins at zero field. The energy (17) has two characteristic values, corresponding roughly to a parallel and an antiparallel orientation of the spin $\mathbf{S}_i$ with respect to $\bar{\mathbf{S}}_j$. With these eigenvalues the partition function ζ_i for the spins of sublattice i is computed. The free energy of the whole system of spins is, then,

$$F = -kT\log Z \quad \text{with} \quad Z = \zeta_i^{N/2}\zeta_j^{N/2}, \quad (18)$$

N being the total number of spins.

To simplify the problem it is now supposed that:

1) C_x, C_y, C_z are small with respect to $|J|$;
2) $\bar{\mathbf{S}}_i$ and $-\bar{\mathbf{S}}_j$ deviate only slightly from an average direction with arbitrarily chosen direction cosines α_i, β_i, γ_i.

The free energy per spin then becomes, in a first approximation and apart from a term independent of α_i, β_i, γ_i,

$$f_{an.} = -(S_o^2/2)(C_x\alpha_i^2+C_y\beta_i^2+C_z\gamma_i^2) \quad (19)$$

where S_o follows from (10).

As $\alpha_i^2 + \beta_i^2 + \gamma_i^2 + 1$, we may write for the anisotropy energy of the whole crystal

$$F = \tfrac{1}{2}(K_1\alpha_i^2 + K_2\beta_i^2) + \tfrac{1}{2}(K_1\alpha_j^2 + K_2\beta_j^2) \qquad (20)$$

where

$$\begin{aligned} K_1 &= N(S_o^2/2)(C_x - C_y) \\ K_2 &= N(S_o^2/2)(C_x - C_z) \end{aligned} \qquad (21)$$

and α_i, βi, and α_j, β_j are direction cosines of $\overline{\mathbf{S}}_i$ and $\overline{\mathbf{S}}_j$. This holds only when $\alpha_i^2 \approx \alpha_j^2$ and $\beta_i^2 \approx \beta_j^2$, i.e. when $\overline{\mathbf{S}}_i$ and $\overline{\mathbf{S}}_j$ are approximately antiparallel.

The temperature dependence is the same as that of S_o^2, and thus the anisotropy energy again disappears at $T = T_N$.

5. *Flop-over of spins, critical field*

We suppose $C_x > C_y > C_z$, and thus $K_2 > K_1 > 0$. Then the x-axis is the preferred direction and the average spin vectors will be directed along the x-axis when $H = 0$. When now an external field is applied in the x,y-plane, the average spin vectors will remain in the x,y-plane too. Indicating with θ the angle between $\mathbf{H}$ and the x-axis and with ψ the angle between $\mathbf{H}$ and the vector $\overline{\mathbf{S}}_i - \overline{\mathbf{S}}_j$ (which has the average direction of alignment), we obtain for the free energy of the system

$$E = -\tfrac{1}{2}\chi_\perp H^2 \sin^2\psi - \tfrac{1}{2}\chi_\parallel H^2 \cos^2\psi + K_1 \sin^2(\theta - \psi). \qquad (25)$$

ψ will be determined from the minimum condition for this expression. Setting the derivative with respect to ψ equal to zero, we obtain

$$\tan 2\psi = \sin 2\theta / (\cos 2\theta - H^2/H_c^2) \quad \text{where} \quad H_c^2 = 2K_1/(\chi_\perp - \chi_\parallel) \qquad (26)$$

This formula, which was given by NÉEL in 1936, describes the flop-over of the spins when $\mathbf{H}$ is directed along the x-axis and passes the critical field H_c. H_c depends upon temperature in a rather complicated wat through K_1 and $\chi_\parallel$.

6. *Theory of GORTER and HAANTJES*[1]

The theory of YOSIDA describes the behaviour of the average spin vectors as a function of temperature and external field in an approximation which is valid when the average spin vectors on both sublattices do not deviate much from the antiparallel posi-

tion, i.e. when the external field is small with respect to the exchange field, and only in the coordinate planes. The theory of GORTER and HAANTJES describes the behaviour of the spin vectors without any limitation on the field strength but only at zero temperature. We will discuss this theory now.

The restriction $T = 0$ simplifies the problem considerably as now the spins in both sublattices will be completely aligned, and each spin vector equals the average spin vector of the corresponding sublattice. We indicate the unit vector parallel to the spin vectors in the first sublattice with $\mathbf{p}^i$, and the analogous vector in the second sublattice with $\mathbf{p}^j$. We will adapt the calculations to a crystal of orthorhombic symmetry and suppose the spins to have an angular momentum $\hbar/2$ in absolute value. Indices 1, 2, 3 will indicate components with respect to the crystal axes. The magnetic moment of an ion in the first and the second sublattice is assumed to be $(\mu_1 p^i_1,\ \mu_2 p^i_2,\ \mu_3 p^i_3)$ and $(\mu_1 p^j_1,\ \mu_2 p^j_2,\ \mu_3 p^j_3)$ respectively. This corresponds to an anisotropic g-tensor, equal for all ions, of which the principal axes coincide with the crystal axes. Thus the presence of two crystallographically different Cu^{2+}-ions in the unit cell of copper chloride and its effect on the g-tensor, as treated by YOSIDA[8], are left unconsidered.

The effective potential energy of a spin i resulting from the interaction with its nearest neighbours is assumed to be

$$\Sigma_k \gamma_k p^i_k p^j_k . \tag{27}$$

This assumption is justified by the formula (17) of YOSIDA. It accounts for the exchange interaction as well as the anisotropy effect. (27) is also the interaction potential energy of the spins j, as (27) is symmetrical in $\mathbf{p}^i$ and $\mathbf{p}^j$. The total interaction energy of the system then is:

$$(N/2)\Sigma_k \gamma_k p^i_k p^j_k \tag{28}$$

where N is the total number of spins. The magnetic energy of the system is

$$-(N/2)\Sigma_k \mu_k p^i_k H_k - (N/2)\Sigma_k \mu_k p^j_k H_k . \tag{29}$$

Thus the complete energy per two spins is

$$E = \Sigma_k (-\mu_k p^i_k H_k - \mu_k p^j_k H_k + \gamma_k p^i_k p^j_k), \tag{30}$$

$$E = -\Sigma_k (h_k p^i_k + h_k p^j_k - \gamma_k p^i_k p^j_k) \tag{31}$$

where $$h_k = \mu_k H_k. \tag{32}$$

The minimum condition for E, $dE=0$ yields

$$\Sigma_k((h_k-\gamma_k p_k^j)\,dp_k^i+(h_k-\gamma_k p_k^i)\,dp_k^j) = 0. \tag{33}$$

As $\mathbf{p}^i$ and $\mathbf{p}^j$ are unit vectors, we have the additional conditions

$$\Sigma_k {p_k^i}^2 = 1, \qquad \Sigma_k p_k^i dp_k^i = 0, \tag{34}$$

$$\Sigma_k {p_k^j}^2 = 1, \qquad \Sigma_k p_k^j dp_k^j = 0. \tag{35}$$

With the Lagrange multiplicators method we obtain from (33, 34, 35)

$$W^i p_k^i = h_k - \gamma_k p_k^j, \tag{36a}$$

$$W^j p_k^j = h_k - \gamma_k p_k^i, \tag{36b}$$

$$\Sigma_k {p_k^i}^2 = 1, \tag{37a}$$

$$\Sigma_k {p_k^j}^2 = 1. \tag{37b}$$

With (36) and (37) the problem is formulated in terms of eight equations with eight unknowns $p_1^i, p_2^i, p_3^i, p_1^j, p_2^j, p_3^j, W^i, W^j$.

Though GORTER and HAANTJES derive equations (36) and (37) in a somewhat different way, their derivation is essentially equivalent to that given here.

As we see from (30), the components of the total effective field, acting on the i-spins, are

$$H_{eff.k}^i = H_k-\gamma_k p_k^j/\mu_k = (h_k-\gamma_k p_k^j)/\mu_k = p_k^i W^i/\mu_k. \tag{38}$$

The magnetic energy of a spin i in this field is

$$-\Sigma_k \mu_k p_k^i H_{eff.k}^i = -W^i. \tag{39}$$

When there is a stable equilibrium, the magnetic moment vector will be orientated parallel to the effective field, corresponding to a negative value of the magnetic energy in the effective field, i.e. to a positive value of W^i. However, the solutions of (36) and (37) will include, also, unstable and metastable equilibria, all having $dE = 0$. The solution corresponding to the situation occurring in nature will be the one with lowest energy, and will at least have positive W^i and W^j.

7. *The solutions of equations (36) and (37)*

We suppose $\gamma_1 > \gamma_2 > \gamma_3$ and use the notation

$$a^2 = \gamma_2^2 - \gamma_3^2, \quad -b^2 = \gamma_3^2 - \gamma_1^2, \quad c^2 = \gamma_1^2 - \gamma_2^2, \quad (b^2 = a^2 + c^2). \tag{40}$$

We introduce the vectors

$$\mathbf{p} = \tfrac{1}{2}(\mathbf{p}^i - \mathbf{p}^j), \tag{41a}$$

$$\mathbf{q} = \tfrac{1}{2}(\mathbf{p}^i + \mathbf{p}^j), \tag{41b}$$

for which, because of (37), the following relations hold:

$$\Sigma_k (p_k^2 + q_k^2) = 1 \quad \text{or} \quad p^2 + q^2 = 1, \tag{41c}$$

$$\Sigma_k p_k q_k = 0 \quad \text{or} \quad \mathbf{p} \perp \mathbf{q}. \tag{41d}$$

With rather complicated mathematical manipulations, GORTER and HAANTJES derive from (36) and (37):

$$C_1 \equiv a^2 p_2 p_3 + (p_1 h_1 + p_2 h_2 + p_3 h_3)(p_2 h_3 - p_3 h_2) = 0, \tag{42}$$

$$C_2 \equiv -b^2 p_3 p_1 + (p_1 h_1 + p_2 h_2 + p_3 h_3)(p_3 h_1 - p_1 h_3) = 0, \tag{43}$$

$$C_3 \equiv c^2 p_1 p_2 + (p_1 h_1 + p_2 h_2 + p_3 h_3)(p_1 h_2 - p_2 h_1) = 0. \tag{44}$$

These equations are not independent, as we have

$$p_1 C_1 + p_2 C_2 + p_3 C_3 = 0. \tag{45}$$

When we consider p_1, p_2, p_3 as homogenous coordinates, (42), (43) and (44) represent three conic sections. Three of the four intersections of $C_1 = 0$ and $C_2 = 0$ have also $C_3 = 0$ because of (45); the fourth intersection has $p_3 = 0$, $p_1 h_1 + p_2 h_2 = 0$. Thus we find, in general, three solutions of the ratio's between p_1, p_2, p_3. It may be shown that the three corresponding directions are perpendicular. From the ratio's of p_1, p_2, p_3 the ratio's of q_1, q_2, q_3 and the absolute values p and q can be computed with (36), (37), (41). The ratio's of p_1, p_2, p_3 and the absolute value p of $\mathbf{p}$ being computed, we obtain two opposite $\mathbf{p}$ vectors, corresponding to trivial interchange of $\mathbf{p}^i$ and $\mathbf{p}^j$. Considering this as one solution, we then have in general three solutions, with mutually perpendicular $\mathbf{p}$ vectors. A fourth solutions is obtained taking $p_1 = p_2 = p_3 = 0$, obviously satisfying (42), (43), (44).

When $h = 0$ the first three solutions give **p** vectors directed along the axes. The solution which has **p** parallel to the x-axis for $h = 0$, will be indicated by A. Similarly we call the solutions with **p** parallel to the y-axis and the z-axis, for $h = 0$, B and C.

Discontinuities in these solutions may occur for those **h** for which (42), (43), (44) do not uniquely define the ratio's of p_1, p_2, p_3. This will be the case when the conic sections $C_1=0$, $C_2=0$, $C_3=0$ either coincide completely or are degenerate and have a common straight line. The former case appears to be a special case of the latter. The degeneration of the curves appears to occur at real values of h_1, h_2, h_3 only when

either $\quad h_2 = 0, \qquad h_1^2/c^2-h_3^2/a^2-1 = 0, \qquad (46)$

or $\quad h_3 = 0, \qquad h_1^2/b^2+h_2^2/a^2-1 = 0. \qquad (47)$

When **h** satisfies (46), solution C is uniquely defined, but the solutions A and B are not. When we let the point of the vector **h** describe a small curve around the hyperbola (46) from one side of the hyperbola in the x,z-plane to the other, the **p**-vectors in in A and B rotate quickly over about $\pi/2$, and thus interchange their directions. The ellipse (47) plays a similar rôle for the B and the C solution. For values of h large with respect to a, b and c, the **p**'s in A and B are approximately perpendicular to **h**, that in C approximately parallel to **h**. When h increases, $\mathbf{p}^i$ and $\mathbf{p}^j$ are, as it were, forced towards the direction of **h**. At a certain value of h, which is about 2γ (the exact value depending on the orientation of **h**), p is zero and $\mathbf{p}^i$ and $\mathbf{p}^j$ are parallel in A and B. For h greater than this critical value A and B become imaginary. Solution C remains real, but the corresponding values of W^i and W^j are negative when $\Sigma_k h_k^2/\gamma_k^2 > 1$.

The fourth solution, with $p = 0$, will be indicated with D. From (36), (37) we have, with $\mathbf{p}^i = \mathbf{p}^j$ and $W^i = W^j$,

$$p_k^i = h_k/(\gamma_k+W^i), \qquad \Sigma_k p_k^{i\,2} = 1. \qquad (48)$$

The condition $W^i \geq 0$ reduces the number of solutions to at most one. This solution exists only when $h \gtrsim \gamma$; for $h < \approx \gamma$, W^i becomes negative. At the value of $h \approx 2\gamma$ at which p becomes zero in A and B, these solutions pass over continuously into D.

The solution with the lowest energy, i.e. the one corresponding to the situation occurring in nature, appears to be solution A as long as it exists, and solution D in the region where A does not exist.

As the ellipse (47) has nothing to do with solution A, only with B and C, it has no physical meaning.

The surface in h-space, which is the boundary between the region where solution A is realised and the region where D is realised will be indicated by Ω. It is defined by $p = 0$ in solution A. The solution A behaves discontinuously when **h** passes the hyperbola (46), which will be indicated by Γ. This discontinuous behaviour corresponds to the flop-over of the spins.

In view of the antiferromagnetic resonance calculations (cf. sec. B. 3) we give here the explicit formulae for the realised solutions when **h** is confined to the coordinate planes.

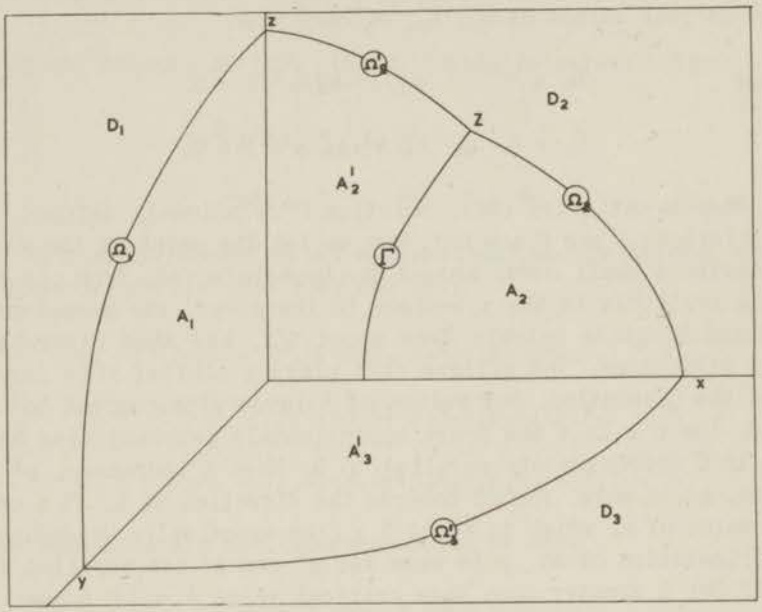

Fig. 2. The regions of application of the static solutions in the coordinate planes of h-space.

8. *The realised solutions in the coordinate planes of h-space*

In the coordinate planes of h-space we have the following regions (cf. fig. 2):

In the x, y-plane the regions A_3' and D_3, separated by Ω_3', where the solutions A and D apply respectively; similarly in the y, z-plane the regions A_1 and D_1 separated by Ω_1 and in the x, z-plane the regions A_2, A_2' separated by Γ, and D_2 separated from A_2 by Ω_2 and from A_2' by Ω_2'.

The explicit formulae for solution A in the regions A_2 and A_2' are different; when those applying in one of these regions are

are analytically continued beyond Γ into the other region we obtain solution B of GORTER and HAANTJES.

The solutions in A_1 and A_2 are characterised by the fact that their **p** is perpendicular to the coordinate plane containing **h**. For solutions in A_2' and A_3', **p** and **h** lie in the same coordinate plane.

In the following, the formulae for Ω_1 and those in A_1 and D_1 are derived from the ones for Ω_2 and those in A_2 and D_2 by interchange of indices 1 and 2; formulae for Ω_3' and in A_3' and D_3 are obtained from those for Ω_2' and in A_2' and D_2 by interchange of indices 2 and 3. In doing this one has to keep in mind that a, b and c, according to (40), contain the indices implicitly.

Solution in A_2. We have $h_2 = 0$, $p_1 = 0$, $p_3 = 0$. From equations (42, 43, 44, 41, 36, 37) we derive

$$q_2 = 0,\ q_1 = h_1/(\gamma_2+\gamma_1),\ q_3 = h_3/(\gamma_2+\gamma_3),$$
$$p_2^2 = 1 - q_1^2 - q_3^2. \tag{49}$$

Solution in A_2'. We have $h_2 = 0$, $p_2 = 0$, $q_2 = 0$. Here polar coordinates are convenient to use. Introducing θ_2, φ_2, ψ_2 as the angle between **h** and the x-axis, **p** and the x-axis, **h** and **p** respectively, we have

$$p_1 = p\cos\varphi_2,\ q_1 = -q\sin\varphi_2,\ h_1 = h\cos\theta_2,\ \psi_2 = \theta_2 - \varphi_2,$$
$$p_3 = \sin\varphi_2,\ q_3 = q\cos\varphi_2,\ h_3 = h\sin\theta_2. \tag{50}$$

Then, from (36) we derive

$$h\sin\psi_2 = q(\gamma_1+\gamma_3), \tag{51}$$

$$2hq\cos\psi_2 + (\gamma_1-\gamma_3)\sin 2\varphi_2 = 0. \tag{52}$$

ψ_2 may be expressed in h and θ_2 by eliminating q and φ_2:

$$\tan 2\psi_2 = b^2\sin 2\theta_2/(b^2\cos 2\theta_2 - h^2). \tag{53}$$

In the following it is convenient to use a variable z_2, defined by

$$z_2^2 = b^4 + h^4 - 2b^2h^2\cos 2\theta_2, \tag{54}$$

$$z_2 \geqq 0. \tag{55}$$

($z_2 = 0$ only for $h_1 = \pm b$, $h_3 = 0$).

Using z_2, the hyperbola (46) may be expressed as

$$z_2 = h^2 + a^2 - c^2. \tag{56}$$

θ_2, ψ_2, φ_2 may be expressed in z_2 with help of (54, 53):

$$\begin{aligned} cos2\theta_2 &= (b^4 + h^4 - z_2^2)/2b^2h^2, \\ cos2\psi_2 &= (b^4 - h^4 - z_2^2)/2h^2z_2, \\ cos2\varphi_2 &= (b^4 - h^4 + z_2^2)/2b^2z_2. \end{aligned} \tag{57}$$

h and θ_2 being given, q and p are found from (53, 51, 50). But, as (53) gives only $tan2\psi_2$, we find two values for ψ_2, corresponding to the A and the C solution; the choice (55) ($z_2 \geqq 0$) pins us down to the A solution. $z_2 \leqq 0$ characterises the C solution.

Solution D. This solution is given by (48), which we write down again:

$$p_k^i = h_k/(\gamma_k + W^i) \quad (k = 1,2,3), \quad \Sigma_k p_k^{i\,2} = 1, \quad W^i \geqq 0. \tag{58}$$

The boundary surface Ω. This is defined by $p = 0$ in solution A.

Ω_2. Taking in (49) $p_2 = 0$ we find the ellipse

$$1 - h_1^2/(\gamma_1 + \gamma_2)^2 - h_3^2/(\gamma_2 + \gamma_3)^2 = 0. \tag{59}$$

Ω_2^I. Taking $q = 1$ in the solution in A_2^I we find with (51, 57) the equation

$$(h^2 + z_2)^2 - b^4 = 4z_2(\gamma_1 + \gamma_3)^2. \tag{60}$$

Ω_2, Ω_2^I and Γ meet in one point Z, which may be seen as follows: With (56), z_2 can be used as a parameter on Γ; on Γ we have

$$h_1^2/c^2 = (z_2 + c^2)/b^2, \quad h_3^2/a^2 = (z_2 - a^2)/b^2. \tag{61}$$

Substituting (61) in Ω_2 (59), and (56) in Ω_2^I (60), we obtain in both cases

$$z_2 = (\gamma_1 + \gamma_2)(\gamma_2 + \gamma_3). \tag{62}$$

9. *Comparison between the theories of YOSIDA and of GORTER and HAANTJES*

The theory of YOSIDA holds only for fields small with respect to the exchange field. Thus, e.g. a solution corresponding to solution D of GORTER and HAANTJES will not be present. On the other hand the theory of GORTER and HAANTJES cannot predict any temperature effects as it is set up for temperature zero.

When we set up conditions such that both theories should apply, we should obtain the same results. These conditions are:

1. $T = 0$, thus $\chi_{\parallel} = 0$ in YOSIDA's theory.
2. Anisotropy energy and magnetic energy small with respect to the exchange energy; thus a, b, c and $h \ll \gamma$ in GORTER and HAANTJES' theory.
3. The g-tensor isotropic; thus $g = 2$ in YOSIDA's theory and $\mu_1 = \mu_2 = \mu_3 = \mu$ in GORTER and HAANTJES' theory.

Under these conditions the following equalities between quantities occurring in both theories hold:

YOSIDA	GORTER and HAANTJES	
$A = 1/\chi_{\perp}$	$= 2\gamma/N\mu^2$,	(63)
$2\lvert J\rvert z + C_k$	$= 4\gamma_k$,	(64)
$2AK_1 \ (= H_c^2)$	$= c^2/\mu^2$,	(65)
$2AK_2$	$= b^2/\mu^2$.	(66)

The behaviour of the magnetization vectors when the external field is confined to the x, y-plane is one of the results which may be seen to be identical in both theories under the mentioned conditions. For then the formula, holding in the x, y-plane, corresponding to (53) in the x, z-plane, is equivalent to (26), YOSIDA's formula.

It may be shown that in the theory of YOSIDA a threshold hyperbola exists, corresponding to the threshold hyperbola of GORTER and HAANTJES, and that it is represented by

$$H_x^2/H_c^2 - H_z^2/H_a^2 - 1 = 0 \tag{67}$$

where H_c and H_a are determined by

$$\alpha H_c^2 = 2AK_1,$$

$$\alpha H_a^2 = 2A(K_2 - K_1), \quad \alpha = 1 - \chi_{\parallel}/\chi_{\perp}.$$

10. *Discussion. Other theories*

The two sublattices molecular field theory, as discussed in the previous sections, predicts a number of features which have been confirmed experimentally in a qualitative way. When we confine our attention to the experimental results on copper chloride $CuCl_2.2H_2O$, the most pronounced of these features are:

1. The existence of a Néel temperature, evident from the

specific heat measurements of FRIEDBERG[10], the susceptibility measurements of VAN DEN HANDEL et.al.[11] and the proton resonance measurements of POULIS et al.[12]. These last measurements give the most accurate determination of T_N, which was found to be $4,33_8{}^{o}K$.

2. The arrangements of the copper ions in two sublattices in such a way that the average magnetic moments in the two sublattices are antiparallel below the Néel temperature. POULIS found that all spins were probably orientated parallel in each a,b-plane, and antiparallel in successive a,b-planes.

3. The temperature dependence of the parallel and perpendicular susceptibility. The experiments of VAN DEN HANDEL et al. confirm the theoretical predictions qualitatively.

4. The existence of a critical field at which the spins flop over from the parallel to the perpendicular orientation when an increasing field is applied in the direction of the a-axis (the preferred direction in copper chloride), evident from the susceptibility measurements as well as the proton resonance measurements.

5. The temperature dependence of the average magnetizations of the sublattices. These should increase from zero to a saturation value when the temperature decreases from T_N to zero. This has been confirmed by POULIS et al.

There remain, however, a number of quantitative discrepancies between the theory under consideration and the experiments. The most important of these are:

1. The relation between the perpendicular susceptibility $\chi_\perp$ and the Néel temperature T_N. These quantities are, according to theory, determined by the exchange interaction. Using (14) and (63) we have $kT_N=\gamma$. The value $10,4.10^{-16}$ erg for γ, obtained from the susceptibility measurements, would lead to a Néel temperature of $7.5^{o}K$, largely different from the measured value $4,33_8{}^{o}K$.

2. The temperature dependence of the average magnetizations of the sublattices. This dependence has been measured by POULIS et al.[12]. Theoretically it should follow from eq.(10), with $S = \frac{1}{2}$ so that $B_S(y_o)$ reduces to $\tanh y_o$. Assuming that the temperature dependence of the specific heat is due to exchange energy only below the Néel temperature, the square of the magnetization of a sublattice is obtained by integrating the specific heat as obtained by FRIEDBERG. Curve 1 in fig. 3 represents the square of the magnetization per sublattice following the measurements of POULIS, curve 2 the same quantity derived from theory and curve 3 as determined from the specific heat. It is seen that they differ strongly. The vertical scales are chosen such that the three curves fit at $T = 0$ and at $T = T_N$. Curve 4 will be discussed in Chapter IV.

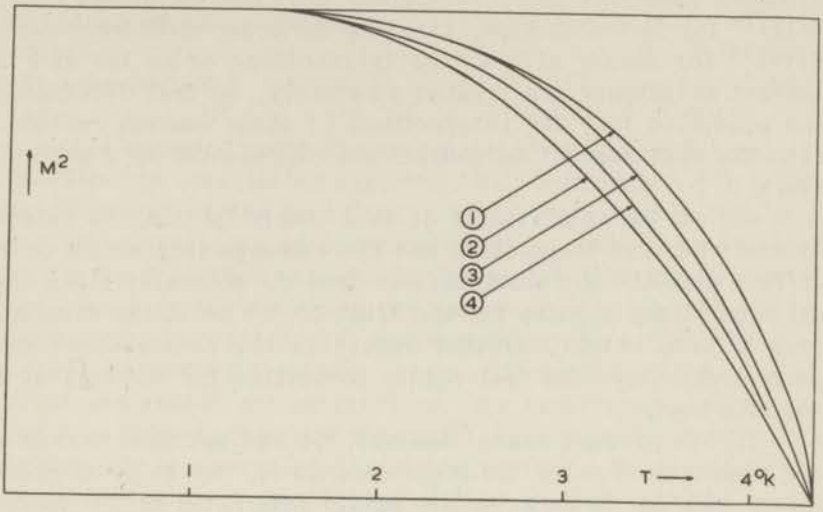

Fig.3. The square of the magnetization per sublattice as a function of temperature.
Curve 1. From the proton resonance measurements of POULIS.
Curve 2. From the molecular field theory with S = ½.
Curve 3. From the specific heat measurements of FRIEDBERG.
Curve 4. From H_c and α (cf. Ch. IV).

3. The large tail of the specific heat above the Néel point as obtained by FRIEDBERG, indicates the persistence of a short range order above The Néel point, which the present theory does not account for.

The molecular field theory has been extended by introducing more than two sublattices. This is necessary when interactions are supposed to exist between nearest neighbours and no division into two sublattices is possible such that all nearest neighbours of an ion in one sublattice belong to the other sublattice. Such a division is not possible e.g. for the face centered cubic lattice and the hexagonal lattice. Cases with more sublattices have been treated by ANDERSON[13], LI[14]. Extensions in this direction, however, are of no use in the case of copper chloride, as here the arrangement in two sublattices seems to be established conclusively.

Another extension of the two sublattices molecular field theory is made by the introduction of an interaction of possibly ferromagnetic character between next nearest neighbours besides the antiferromagnetic interaction between nearest neighbours[2,13].

A theory which should describe antiferromagnetism in a better approximation than the molecular field theory is the order-

disorder theory of LI[15]. It follows the lines developed by P.R. WEISS[16] for ferromagnetism, based on the order-disorder theory of BETHE[17] for binary alloys. The interactions of an ion with its nearest neighbours are treated separately, so that fluctuations are accounted for. The interactions of these nearest neighbours with the next nearest neighbours are represented by a molecular field.

One of the main results of this theory is that the relation between the Néel temperature and the exchange interaction energy differs from the one which follows from the molecular field theory. Thus it may account for the first of the mentioned discrepancies to some extent. Another result is the existence of short range order above the Néel point, accounting for the tail of the specific heat.

In its present state, however, it has not been worked out for temperatures below the Néel temperature. Thus it is at present not of much use to us as we are mainly interested in the temperature region between zero and the Néel temperature.

Another and more fundamental approach to describing antiferromagnetism is made in the spin wave theory[18,19,20,21]. Here, an approximation is used in which the spins are supposed to deviate only slightly from their antiparallel alignment along a preferred direction, thus the results hold only for temperatures near zero and small external fields. In the quantummechanical attack the spin operators are transformed into other operators such that the Hamiltonian may more easily be diagonalised. One of the most characteristic results is that the sublattices are not completely saturated at temperature zero.

Both the order-disorder theory and the spin wave theory should give more correct results than the molecular field theory. Nevertheless we will confine our discussions in the following parts to the molecular field theory, because the theories mentioned above in their present state are limited to rather narrow ranges of temperature and magnetic field due to their basic approximations.

B. Antiferromagnetic resonance

1. *Introduction*

When a magnetic substance is subjected to a constant magnetic field and an oscillating magnetic field, absorption of electromagnetic energy of the oscillating field may occur in the substance. This thesis is concerned with the *resonance* absorption, which may be described classically by saying that the system of magnetic ions in the substance may have one or more characteristic modes of oscillation with corresponding characteristic frequencies, depending upon the external constant field. Due to interactions, which act as friction, the oscillations, once set up, will be damped. When now the oscillating magnetic field has a frequency close to one of the characteristic frequencies the corresponding mode of oscillation will be excited, and the system of magnetic ions comes into resonance with the oscillating field. Due to the friction, work will be done by the alternating field to keep the system oscillating, which results in the resonance absorption.

The corresponding quantummechanical picture of the resonance phenomenon is that the oscillating field may induce transitions between energy levels of the system of magnetic ions which are separated by an energy h times the frequency of the oscillating field. When such pairs of energy levels are present, which depends upon the external constant field, and when transitions between these levels are allowed, resonance will occur.

1.1. *One spin.* Some characteristic features of the resonance phenomenon are clearly shown when we consider one spin in a magnetic field. The angular momentum of the spin is $\hbar\mathbf{S}$, and $S = \frac{1}{2}$. The magnetic moment is $\mathbf{M} = g\beta\mathbf{S}$, where β is the Bohr magneton and g the Landé factor, in this case equal to 2. The magnetic energy of the spin in the constant magnetic field $\mathbf{H}$ then is

$$-(\mathbf{MH}) = -g\beta\,(\mathbf{SH}). \tag{1}$$

In the quantummechanical treatment the characteristic values of this energy are determined. They are $E = \pm \frac{1}{2}g\beta H$, corresponding to a parallel and an antiparallel orientation of $\mathbf{S}$ with respect to $\mathbf{H}$. The energy separation is $\Delta E = g\beta H$. Transitions between the levels, i.e. the turning over of the spin, will imply absorption or emission of a photon with energy

$$h\nu = g\beta H. \tag{2}$$

The photon corresponds to electromagnetic energy in the oscillating field with frequency ν. (2) is the resonance condition, i.e. the relation between H and ν for which resonance occurs.

Treating the oscillating field as a perturbation, the probability of a transition induced by it, may be calculated. This results in the fact that the probability is zero when the oscillating field is parallel to the constant field. In other words, only the components of the oscillating field perpendicular to the constant field induce transitions.

Treating the problem classically we write down the equation of motion for the spin which states that the time derivative of the angular momentum equals the torque acting on the spin. When we write $\gamma = g\beta/h$, then the angular momentum is $\mathbf{M}/\gamma$, and the equation of motion is

$$(1/\gamma)\ d\mathbf{M}/dt = [\mathbf{M} \times \mathbf{H}]. \qquad (3)$$

Suppose first we have only a constant magnetic field which is directed along the z-axis; $H_x = H_y = 0$, $H_z = H$. We then have

$$dM_x/dt = \gamma M_y H, \quad dM_y/dt = -\gamma M_x H, \quad dM_z/dt = 0. \qquad (4)$$

The static solution is the one in which the time derivatives equal zero. We obtain the trivial solution

$$M_x = M_y = 0, \quad M_z = \pm M. \qquad (5)$$

$M_z = +M$ corresponds to the stable equilibrium.
By integrating equations (4) we obtain the oscillating solution

$$M_x = M_o exp(\pm i\omega_o t), \quad M_y = \pm iM_o exp(\pm i\omega_o t), \quad M_z = constant, \qquad (6)$$

where

$$\omega_o = \gamma H. \qquad (7)$$

(6) describes the Larmor precession, and (7) gives the Larmor frequency. (7) is the resonance condition and equivalent to (2).

Suppose now an oscillating field $\mathbf{h}$ is superposed on the static field and consider its effect on the static solution (5). The components of the magnetic moment will deviate from those in (5); let the deviation be $\mathbf{m}$. We suppose m and h to be small relative to M and H and adopt only first order terms in the components of m and h in the equations of motion. It is seen, then, that h_z does not appear in the first order equations. This means that an oscillating field parallel to the constant field does not excite oscillation of the spin. When we now substitute

$$h_x + ih_y = h_o exp(- i\omega t),$$
$$h_x - ih_y = h_o exp(+ i\omega t), \tag{8}$$

which means that the x,y-part of the oscillating field has a circular polarization, the first order equations are solved with

$$m_x + im_y = m_o exp(- i\omega t),$$
$$m_x - im_y = m_o exp(+ i\omega t), \tag{9}$$
$$m_z = 0,$$

where

$$m_o = \gamma h_o M/(\omega_o - \omega), \tag{10}$$

except for additive terms of the type (6) which give the free oscillation. From (10) we may derive a „radio frequency susceptibility" $\chi_{rf} = m_o/h_o$ and we have

$$\chi_{rf} = \gamma M/(\omega_o - \omega). \tag{11}$$

Thus the χ_{rf} is real when $\omega \neq \omega_o$, and it shows a dependence upon the frequency which is typical for dispersion.

1.2. *More spins.* When we have a system of spins, completely independent from their surroundings and from each other, we may treat them separately as done above. In nature, however, the magnetic ions are immersed in crystals, and the non magnetic parts of the crystals will, in general, generate electric fields at the positions of the ions, and thus influence them. Moreover, magnetic ions will always interact with each other.

The influence of the surroundings will have the following effects:

1) In the classical picture it introduces friction terms and thus the alternating field has to do work to keep the system oscillating, which results in absorption. In the quantummechanical picture this corresponds to the fact that the interaction keeps the distribution over the energy levels constant. Suppose two energy levels with energies E_1 and E_2 ($E_1<E_2$) have populations N_1 and N_2 ($N_1>N_2$). The oscillating field with frequency $(E_2 - E_1)/h$ induces transitions between these levels with apriori equal probabilities for the transition $E_1 \rightarrow E_2$ and the transition $E_2 \rightarrow E_1$. Thus the number of transitions $E_1 \rightarrow E_2$, which imply absorption, is proportional to N_1 and the number of transitions $E_2 \rightarrow E_1$, which imply emission, is proportional to N_2, and there is a net absorption proportional to $N_1 - N_2$. If no interactions were present, N_1

and N_2 would become equal, and the system would cease to absorb.

2) In a crystal equivalent magnetic ions will be acted upon by equal crystalline fields. These fields will change the pattern of the energy levels as a function of the magnetic field, and thus change the field at which resonance occurs. When the spin quantum number is larger than ½, this may give rise to several resonance fields. Information about the crystalline fields may be obtained by the study of these multiple resonance fields, which is an important purpose of paramagnetic resonance experiments. This effect may sometimes conveniently be described by the introduction of an anisotropic g-tensor.

3) The thermal motion of the crystal lattice will blur the energy levels which results in thermal broadening of the magnetic resonance lines.

The mutual interaction of the magnetic ions may generally be described by means of a local field, which is the magnetic field generated by the surrounding ions at the position of one ion. It may be a true magnetic field, when we consider the magnetic interactions, or a virtual magnetic field, e.g. when we consider exchange interaction. Fluctuations in the local fields will cause magnetic broadening of the resonance lines. In cases where it is justified to adopt the Weiss molecular field approximation, i.e. to set equal the local fields for all ions of a certain system (e.g. the magnetic ions of one sublattice in an antiferromagnetic crystal), we obtain by adding this local field to the external field a total effective field which is equal for all ions of the system. We then may take the averages in eq.(3) and obtain the equation of motion for the average magnetization of this system of ions

$$(1/\gamma)\ d\mathbf{M}/dt = [\mathbf{M} \times \mathbf{H}_{eff.}] \qquad (12)$$

where $\mathbf{M}$ is the average magnetic moment of the system of ions and $\mathbf{H}_{eff.}$ is the sum of the external and average local field.

When equation (12) is applied to the paramagnetic case, the Weiss local field drops out of the equation, as this field is always parallel to $\mathbf{M}$, and thus its vector product with $\mathbf{M}$ equals zero. Therefore, eq.(12) may be applied to the paramagnetic case with $\mathbf{H}_{eff.} = \mathbf{H}$, the external field, apart from a correction for a possible anisotropic g-tensor (sec.1.3).

In the antiferromagnetic case two equations of the type (12), one for each sublattice, are used to determine the resonance frequency.

1.3. *Anisotropic g-tensor.* An anisotropic g-tensor means

that the relation between the magnetic moment **M** and the angular momentum **I** is anisotropic. This may be taken into account by introducing, instead of the magnetomechanical ratio γ, a tensor $\boldsymbol{\gamma}$, such that $\mathbf{M} = \boldsymbol{\gamma}\,\mathbf{I}$. When as axes are taken the principal axes of **g** or $\boldsymbol{\gamma}$, this equivalent to

$$M_k = \gamma_k\, I_k. \tag{13}$$

The magnetic energy is

$$-(\mathbf{M}\,\mathbf{H}) = -\Sigma_k M_k H_k = -\Sigma_k \gamma_k I_k H_k. \tag{14}$$

From (14) it is seen that the system behaves as one with an angular momentum **I**, a magnetomechanical ratio 1, placed in a field with components $\gamma_k H_k$. Thus, we obtain, instead of (12), as the equation of motion

$$d\mathbf{I}/dt = [\mathbf{I} \times (\boldsymbol{\gamma}\,\mathbf{H}_{eff.})]. \tag{15}$$

We are mainly interested in the resonance condition in an antiferromagnetic substance, which we will discuss in the next sections. Other problems like line widths, dispersion, polarization will not be treated or only very summarily.

1.4. *The resonance condition in antiferromagnetism.* The resonance condition is obtained by solving two equations of the type (12) or (15), one for each sublattice. In $\mathbf{H}_{eff.}$ for one sublattice the average magnetization of the other sublattice will appear. The resonance frequencies are the frequencies of the harmonically oscillating solutions.

The straight forward method to determine the resonance frequency is as follows:

Take the first order equations in the variations of the static solutions which follow from the equations of motion and suppose these variations to be harmonically dependent upon time. These equations are homogenous in the variations, thus, to have solutions, the determinant of the coefficients of the variations has to be zero. The elements of the determinant contain the frequency (from the time derivative) and the static solutions; expressing the latter in terms of the external field the equating of the determinant to zero yields the resonance condition.

We will review in the following the calculations of YOSIDA[22], adapted to copper chloride, and our own calculations[23], based on the static solutions of GORTER and HAANTJES. YOSIDA's calcula-

tions include non zero temperatures, but are confined to fields small with respect to the exchange fields. In our calculations the case is reversed. The results of NAGAMIYA[24] which are confined to small deviations of the magnetizations from the preferred axis, can be obtained as a special case of YOSIDA's result. KEFFER and KITTEL[25] introduce a somewhat more general macroscopic energy than done by YOSIDA in the case of orthorhombic symmetry.

2. *The resonance condition derived by YOSIDA[22], applying to copper chloride*

YOSIDA derives the resonance condition for the case of copper chloride following the straight forward method indicated above, using as a basis the solutions of the static problem discussed in sec. A.4 and 5. He neglects the anisotropy of the g-tensor, and confines the calculations to the x,y-plane (the x-axis is the easiest and the y-axis the next easiest axis of magnetization).

The static solutions for the magnetization vectors are obtained by adding to the magnetization vectors at zero field, $+\mathbf{M}_o$ and $-\mathbf{M}_o$, the vectors $\frac{1}{2}\chi_{\parallel}\mathbf{H}_{\parallel}$ and $\frac{1}{2}\chi_{\perp}\mathbf{H}_{\perp}$, where $\parallel$ and $\perp$ refer to directions with respect to M_o. Thus we have

$$M_x^i = (M_o + \tfrac{1}{2}\chi_{\parallel} H\cos\psi)\cos(\psi-\theta) + \tfrac{1}{2}\chi_{\perp} H \sin\psi \sin(\psi-\theta) \qquad (16)$$

and similar expressions for M_y^i, M_x^j, M_y^j. ψ has to be determined from sec. A.5 eq. (26).

The torques, appearing in the equations of motion, consist of:

1) the torques arising from the external field: $[\mathbf{M}^{i,j}\times\mathbf{H}]$;
2) the torques arising from the exchange fields $-[\mathbf{M}^{i,j}\times A\mathbf{M}^{j,i}]$; $-A\mathbf{M}^{j,i}$ are the exchange fields; when H is small with respect to the exchange field we have $H_{\perp}/H_{exch} = \delta M_{\perp}/M_o = \chi_{\perp}H_{\perp}/M_o$, thus $A = 1/\chi_{\perp}$;
3) the torques arising from the anisotropy energy sec.A. 4, eq. (20), which are

$$[-(K_2-K_1)M_z^{i,j}M_y^{i,j}/M_o^2,\ K_2M_x^{i,j}M_z^{i,j}/M_o^2,\ -K_1M_x^{i,j}M_y^{i,j}/M_o^2]. \qquad (17)$$

Neglecting K_1/M_0 and K_2/M_0 with respect to AM_0 (i.e. the anisotropy energy with respect to the exchange energy), YOSIDA finds the resonance condition to be:

$$(\omega/\gamma)^4 - (\omega/\gamma)^2[H^2(\alpha^2\cos^2\psi + 1) + 2AK_2 - 2AK_1\{2\sin^2(\psi-\theta) -$$

$$\cos^2(\psi-\theta)\}] + \alpha^2H^4\cos^2\psi - H^2[2AK_1\{\cos\theta\sin\psi\sin(\psi-\theta) +$$

$$\alpha\cos^2\psi\cos2(\psi-\theta) + \alpha\sin\theta\cos\psi\sin(\psi-\theta)\} + 2AK_2(\alpha\cos^2\psi - \sin^2\psi)] +$$

$$+ 2AK_1\cos2(\psi-\theta)[2AK_2 - 2AK_1\sin^2(\psi-\theta)] = 0. \qquad (18)$$

Here ψ has still to be determined from sec.A.5 eq.(26) and $\alpha = 1 - \chi_{\parallel}/\chi_{\perp}$.

When **H** *is directed along the x-axis,* then $\theta = 0$, and $\psi = 0$ when $H < H_c$, $\psi = \pi/2$ when $H > H_c$. The resonance condition then reduces to

$$(\omega/\gamma)^4 - (\omega/\gamma)^2[H^2(1+\alpha^2)+2A(K_1+K_2)]+(\alpha H^2-2AK_1)(\alpha H^2-2AK_2) =0 \quad (19)$$

for $H < H_c$,

$$((\omega/\gamma)^2 + 2AK_1 - 2AK_2)((\omega/\gamma)^2 - H^2 + 2AK_1) = 0 \quad \text{for} \quad H > H_c \quad (20)$$

When **H** is directed along the y- or z-axis, we always have $\psi = 0$ and relations are obtained similar to (20). The temperature dependence of the resonance frequency arises from the temperature dependence of K_1, K_2 and α. Moreover, the regions where (19) or (20) hold are temperature dependent since H_c varies with temperature. We will postpone the discussion of these temperature dependencies till Chapter IV.

3. *The resonance condition derived on the basis of the static solutions of* GORTER *and* HAANTJES

We adopt the notations of Sections A. 6, 7, 8. The resonance condition is a relation between the frequency and the external field, and thus may be represented by a surface in field space for each value of the frequency. We will calculate the intersections of the corresponding surfaces in the h-space (h being defined by A.6, (32)) with the coordinate planes. From this we will get a picture of how these surfaces behave as a function of the frequency.

The equations of motion become, when we take into account the anisotropy of the g-tensor (cf.sec.1.3),

$$(\hbar/2)\, d\mathbf{p}^i/dt = [\mathbf{p}^i \times (\mu\mathbf{H}^i_{eff})]. \qquad (21)$$

Substituting in this the effective field (A.6, (38)) we obtain

$$(\hbar/2)dp_1^i/dt = p_2^i(h_3 - \gamma_3 p_3^j) - p_3^i(h_2 - \gamma_2 p_2^j) \qquad (22)$$

and similar expressions for the other components and the other sublattice. Transforming these equations to those for the sum and difference vectors **p** and **q** (A.7, (41)) we obtain

$$\begin{aligned}(\hbar/2)dp_1/dt &= p_2h_3 - p_3h_2 - (\gamma_2 + \gamma_3)(p_2q_3 - p_3q_2),\\ (\hbar/2)dq_1/dt &= q_2h_3 - q_3h_2 - (\gamma_2 - \gamma_3)(p_2p_3 - q_2q_3).\end{aligned} \qquad (23)$$

Following the straight forward method to obtain the resonance condition from these equations of motion, the determinant to be equated to zero is

$$\Delta = \begin{vmatrix} -i\varepsilon & G_{32} & -G_{23} & 0 & L_{32} & -L_{23} \\ -G_{31} & -i\varepsilon & G_{13} & -L_{31} & 0 & L_{13} \\ G_{21} & -G_{12} & -i\varepsilon & L_{21} & -L_{12} & 0 \\ 0 & -L_{32}' & -L_{23}' & -i\varepsilon & G_{32}' & -G_{23}' \\ -L_{31}' & 0 & L_{13}' & -G_{31}' & -i\varepsilon & G_{13}' \\ L_{21}' & -L_{12}' & 0 & G_{21}' & -G_{12}' & -i\varepsilon \end{vmatrix} \qquad (24)$$

where $G_{kl} = h_k - (\gamma_k + \gamma_l)q_k$, $\quad L_{kl} = (\gamma_k + \gamma_l)p_k$,

$G_{kl}' = h_k - (\gamma_k - \gamma_l)q_k$, $\quad L_{kl}' = (\gamma_k - \gamma_l)p_k$, $\quad \varepsilon = \hbar\omega/2.$

(25)

ω is the circular frequency of the oscillating parts of the magnetization vector. Keeping in mind the relations between the variations of the p_k and q_k following from variation of the relations A(41, c, d), Δ may be reduced to the following lower order determinant

$$\Delta = \frac{-\varepsilon^2}{\beta_{12}^4} \begin{vmatrix} -\beta_{12}i\varepsilon + d_{321}' & -\beta_{12}L_{21}' - d_{121} & -d_{321} & -\beta_{21}L_{12}' - d_{221} \\ e_{123}' & -\beta_{12}i\varepsilon + \alpha_{11}L_{32} & \beta_{12}G_{23} + \alpha_{13}L_{32} & \beta_{21}G_{32} + \alpha_{12}L_{32} \\ e_{321}' & -\beta_{12}G_{21} - e_{121} & -\beta_{12}i\varepsilon - e_{321} & -\beta_{12}G_{12} - e_{221} \\ e_{213}' & \beta_{12}G_{31} + \alpha_{21}L_{32} & \beta_{21}G_{13} + \alpha_{23}L_{31} & \beta_{21}i\varepsilon + \alpha_{22}L_{31} \end{vmatrix}$$

(26)

where

$$\begin{aligned} e_{klm}' &= \beta_{kl}L_{lm} + \beta_{km}L_{ml},\\ e_{klm} &= \alpha_{kl}L_{lm} + \alpha_{km}L_{ml},\\ d_{klm} &= \alpha_{kl}G_{lm}' + \alpha_{km}G_{ml}',\\ d_{klm}' &= \beta_{kl}G_{lm}' + \beta_{km}G_{ml}' \end{aligned} \qquad (27)$$

and

$$\alpha_{kl} = p_k p_l - q_k q_l,$$
$$\beta_{kl} = p_k q_l - p_l q_k. \tag{28}$$

In (24) and (26) the indices may be interchanged. In special cases the indices are chosen in the most favourable way, e.g. such that the β_{kl} occurring in the denominator in (26) does not vanish.

3.1. *Formulae in the coordinate planes.* Confining our attention now to the coordinate planes in h-space and to the realised static solutions, we substitute in (26) the solutions obtained in Sec.A.8. The following expressions are obtained:

Region A_2:
$$-\Delta/\varepsilon^2 = \varepsilon^4 + B_2\varepsilon^2 + C_2 \tag{29}$$

where
$$B_2 = 2[\Upsilon_1\Upsilon_3 - \Upsilon_2^2 - \Upsilon_3 h_1^2/(\Upsilon_1+\Upsilon_2) - \Upsilon_1 h_3^2/(\Upsilon_2+\Upsilon_3)], \tag{30}$$

$$C_2 = -a^2c^2(1-h_1^2/c^2+h_3^2/a^2)[1 - h_1^2/(\Upsilon_1+\Upsilon_2)^2 - h_3^2/(\Upsilon_2+\Upsilon_3)^2]. \tag{31}$$

Region A_2':
$$-\Delta/\varepsilon^2 = \varepsilon^4 + B_2'\varepsilon^2 + C_2' \tag{32}$$

One of the simplest expressions for B_2' is

$$B_2' = h^4 \sin^2 2\psi/(\Upsilon_1+\Upsilon_3)^2 - h^2[\Upsilon_1+\Upsilon_2+\Upsilon_3+(\Upsilon_1+\Upsilon_3-\Upsilon_2)\cos 2\psi_2]/(\Upsilon_1+\Upsilon_3)$$
$$- (\Upsilon_1-\Upsilon_3)(\Upsilon_1+\Upsilon_2+\Upsilon_3)\cos 2\varphi_2 - \Upsilon_1(\Upsilon_1-\Upsilon_2) + \Upsilon_3(\Upsilon_2-\Upsilon_3) \tag{33}$$

and for C_2':
$$C_2' = \tfrac{1}{2}p^2 z_2(z_2 - h^2 - a^2 + c^2). \tag{34}$$

Solution D: The expression for Δ in (24) becomes relatively simple without being restricted to the coordinate planes; as all L_{kl} and $L_{kl}' = 0$, it factorises and we have

$$\Delta/\varepsilon^2 = \Delta_1\Delta_2, \tag{35}$$

$$\Delta_1 = -\varepsilon^2 + p_1'^2(W'+\Upsilon_2)(W'+\Upsilon_3) + p_2'^2(W'+\Upsilon_3)(W'+\Upsilon_1) + p_3'^2(W'+\Upsilon_1)(W'+\Upsilon_2), \tag{36}$$

$$\Delta_2 = -\varepsilon^2 + p_1'^2(W'-\Upsilon_2)(W'-\Upsilon_3) + p_2'^2(W'-\Upsilon_3)(W'-\Upsilon_1) + p_3'^2(W'-\Upsilon_1)(W'-\Upsilon_2). \tag{37}$$

3.2. *The resonance condition at zero frequency.* For $\varepsilon = 0$ we find in the different cases:
A_2: We have from (29): $C_2=0$. Setting the first factor in C_2 equal to zero yields Γ, the second yields Ω_2 (cf.sec.A.8).
A_1: Setting equal to zero the factor corresponding to the first

one in C_2 yields an imaginary ellipse, and the factor corresponding to the second in C_2 yields Ω_1.

A_2': $C_2' = 0$ gives:

1) $p = 0$ which yields Ω_2'.
2) $z_2 = 0 \rightarrow (b,0,0)$, this is a point outside region A_2', thus it does not apply.
3) $z_2 = h^2 + a^2 - c^2 \rightarrow \Gamma$.

A_3': 1) $p = 0 \rightarrow \Omega_3'$.
2) $z_3 = 0 \rightarrow (c,0,0)$, the intersection of Γ with the x-axis.
3) $z_3 = h^2 - a^2 - b^2$; this condition is never satisfied in A_3': squaring both sides yields an ellipse, but on this ellipse $z_3 < 0$ in contradiction with the assumption corresponding to A(55).

D: For $\varepsilon = 0$, Δ_1 is always positive, thus $\Delta_2 = 0$ remains. In D_2 we have, with $\varepsilon = 0$, $h_2 = 0$, $p_2' = 0$:

$$(W'-\gamma_2)[(W'-\gamma_3)p_1'^2 + (W'-\gamma_1)p_3'^2] = 0 \qquad (38)$$

1) $W' = \gamma_2$; with A(58) this results in the ellipse A(59); only the part Ω_2 applies, the other part (on the other side of Γ) lies in the region A_2'.
2) $(W' - \gamma_3)p_1'^2 + (W' - \gamma_1)p_3'^2 = 0.$ (39)
With A(58) this results in

$$h_1^2 = (\gamma_1 - W')(W' + \gamma_1)^2/(\gamma_1 - \gamma_3),$$
$$h_3^2 = (W' - \gamma_3)(W' + \gamma_3)^2/(\gamma_1 - \gamma_3). \qquad (40)$$

This defines a curve on which W' has to be considered as a parameter. Expressing z_2 with A(54) and (40) in W' we get

$$z_2 = (W' + \gamma_1)(W' + \gamma_3). \qquad (41)$$

Substituting (41) and (40) in A(60), the last equation is identically satisfied, thus A(60) and (40) are identical; again only Ω_2' applies, the other part lying in the region A_2.

In D_1 and D_3 we find the analogues of A(59) and A(60). In D_1 the analogue of A(60) lies within that of A(59), and only Ω_1 applies. In D_3 the case is just reversed and only Ω_3' applies.

Resuming: For $\varepsilon = 0$ the resonance condition reduces to Γ and Ω at least in the coordinate planes. We might expect to find Γ, as $\Delta = 0$ for $\varepsilon = 0$ means that first order variations of $\mathbf{p}$ and $\mathbf{q}$ are possible when $\mathbf{h}$ does not vary. This is clearly true for $\mathbf{h}$ on Γ as $\mathbf{p}$ and $\mathbf{q}$ are not uniquely determined there. That Ω satisfies $\Delta = 0$ for $\varepsilon = 0$ might also be predicted: when $\Delta \neq 0$ (with $\varepsilon = 0$), there is only one solution for the δp_k and δq_k when the δh_k are

given; on Ω we have mathematically two solutions corresponding to the solutions A and D, thus must $\Delta = 0$ on Ω.

3.3. *The resonance fields parallel to the axes as functions of the frequency.* When $h_2 = h_3 = 0$, the curves in fig.4 represent the remaining relation between h_1 and ε. The points $h_1 = c$ and $h_1 = \gamma_1 + \gamma_2$ on the h_1-axis correspond to the intersections of the x-axis with Γ and Ω.

The two curves for $h_1 < c$ are branches of a curve of the fourth degree in ε and h_1 representing (32) with $\Delta = 0$, $h = h_1$, $\psi_2 = \varphi_2 = 0$, $z_2 = b^2 - h_1^2$, $p = 1$. The two curves for $c < h_1 < \gamma_1 + \gamma_2$ are parts of an ellipse and of an hyperbola, in which (29) with $\Delta = 0$ may be factored for $h_3 = 0$. The resonance condition in $A_3^!$ for $h = h_1$, $\theta_3 = 0$ should have the same result in both cases, which is easily verified.

The two curves for $h_1 > \gamma_1 + \gamma_2$ are each part of a hyperbola, the lower and the higher branch representing $\Delta_2 = 0$ and $\Delta_1 = 0$ from (37) and (36) respectively, with $h_2 = h_3 = 0$.

For the coordinates of characteristic points see table I (p. 45).

The analogous diagrams when **h** is directed along the y- or the z-axis have in the A-solution only an ellipse and a hyperbola which, when **h** is parallel to the y-axis, intersect in a point

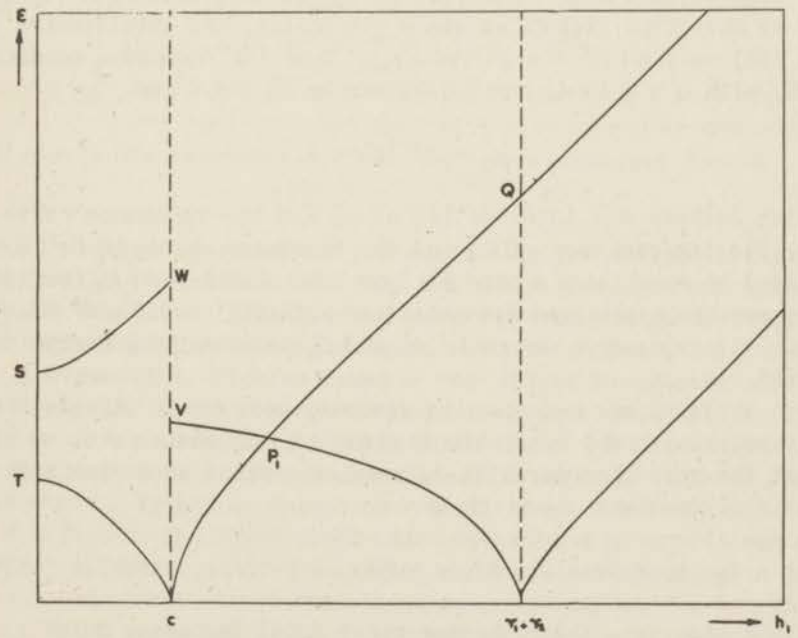

Fig.4. The resonance condition along the h_1-axis.

P_2 ($h_2 = \sqrt{(\gamma_1 + \gamma_2)(\gamma_2 \quad \gamma_3)}$, $\varepsilon = b$) and do not intersect when **h** is parallel to the z-axis.

3.4. *Properties of the resonance surface on* Ω *and* Γ. As the static solutions are continuous when **h** passes Ω, we may expect the resonance surfaces inside and outside Ω to meet on Ω. This may be confirmed in the coordinate planes:

Intersecting the resonance condition in A_2 with Ω_2, i.e. solving (29) with $\Delta = 0$ and A(59) for h_1^2 and h_3^2 gives:

$$\begin{aligned} \gamma_2(\gamma_1 - \gamma_3)h_1^2/(\gamma_1 + \gamma_2)^2 &= \gamma_2(\gamma_1 + \gamma_2) - \tfrac{1}{2}\varepsilon^2, \\ \gamma_2(\gamma_1 - \gamma_3)h_3^2/(\gamma_2 + \gamma_3)^2 &= \tfrac{1}{2}\varepsilon^2 - \gamma_2(\gamma_2 + \gamma_3). \end{aligned} \tag{42}$$

The resonance curve in D_2 resulting from $\Delta_1 = 0$ with $h_2 = 0$ may be described with a parameter W. We have from (36) and A(58), substituting W for W',

$$\begin{aligned} (\gamma_1 - \gamma_3)h_1^2 &= (W + \gamma_1)^2[W + \gamma_1 - \varepsilon^2/(W + \gamma_2)], \\ (\gamma_3 - \gamma_1)h_3^2 &= (W + \gamma_3)^2[W + \gamma_3 - \varepsilon^2/(W + \gamma_2)]. \end{aligned} \tag{43}$$

Taking in (43) $W = \gamma_2$ we just find (42), i.e. the resonance curve in D_2 intersects Ω_2 in the same point as the resonance curve in A_2 does.

As we have seen in sec. 3.2 Ω_2' may be described with (40). On Ω_2' we have from (34) $C_2' = 0$ (as $p = 0$ on Ω_2'), and substituting (40) in (33) we find $B_2' = -2W'(W' + \gamma_2)$. Thus the resonance condition (32) with $\Delta = 0$ in A_2' on Ω_2' is given by $B_2' = -\varepsilon^2$ or

$$\varepsilon^2 = 2W'(W' + \gamma_2) \tag{44}$$

which defines the intersection of Ω_2' and the resonance curve in A_2'. The intersection of Ω_2' and the resonance curve in D_2 is obtained by equalizing h_1^2 and h_3^2 from (40) with h_1^2 and h_3^2 from (43). The equations obtained are satisfied with $W = W'$ and $\varepsilon^2 = 2W'(W' + \gamma_2)$; thus the resonance curves in A_2' and D_2 intersect Ω_2' in the same point.

The resonance surface is discontinuous on Γ. Using z_2 as a parameter on Γ and substituting A(61) in (29) with $\Delta = 0$, we find that the resonance curve in A_2 reaches a point on Γ with a given z_2 for a frequency ε_2 given by

$$\varepsilon_2^2 = 2\gamma_2[z_2 + (\gamma_1 - \gamma_2)(\gamma_2 - \gamma_3)]/(\gamma_1 + \gamma_3). \tag{45}$$

In the same way, the resonance curve in A_2' reaches a point z_2 on Γ at a frequency ε_2' given by

$$\varepsilon_2'^2 = \varepsilon_2^2\{1 + 2a^2c^2[(\gamma_1 + \gamma_2)(\gamma_2 + \gamma_3) - z_2]/\gamma_2(\gamma_1 + \gamma_3)z_2^2\}. \quad (46)$$

The point Z on Γ was given by A(62): $z_2 = (\gamma_1 + \gamma_2)(\gamma_2 + \gamma_3)$. For this value of z_2 we have from (46) $\varepsilon_2' = \varepsilon_2$ and from (45) $\varepsilon_2 = 2\gamma_2$. That is, the intersections of the resonance curves in A_2' and A_2 with Γ reach Z for the same frequency, given by $\varepsilon = 2\gamma_2$. At this frequency Z is also reached by the intersection of Ω_2 and the resonance curve in A_2, as may be verified with help of (42) and A(59).

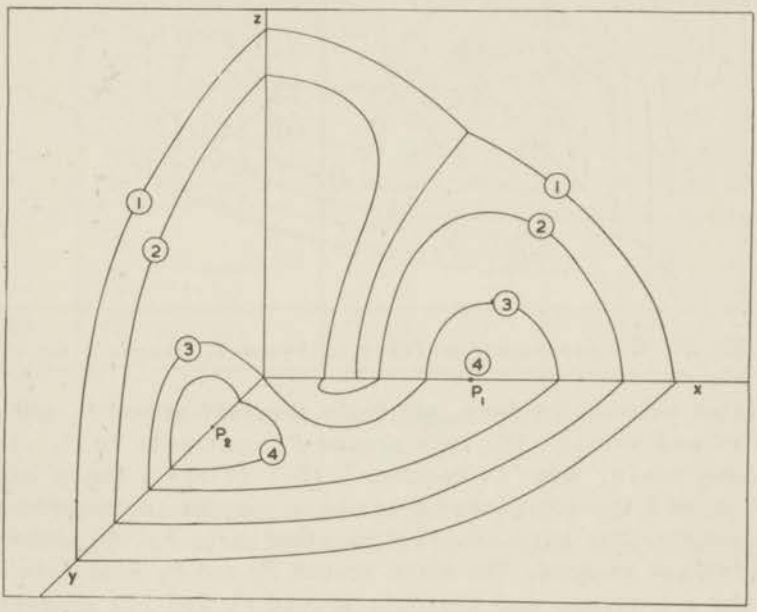

Fig.5. The resonance surfaces in h-space. Stages 1 to 4.

3.5. *The resonance surfaces for increasing frequency.* Combining the results of sections 3.2, 3.3, 3.4 with a few numerical calculations based on section 3.1, we come to the following description of the surfaces representing the resonance condition in h-space for increasing ε. Figures 5 and 6 show the intersections of the surfaces with the coordinate planes for several values of ε. The values of ε, corresponding to critical stages of the development of the resonance surfaces, are given in Table I. For $\varepsilon = 0$ we have Ω and Γ (stage 1). When ε increases, the surface representing $\Delta_2 = 0$ (not in the figures) expands regularly, and we will pay no further attention to it. The other surface, corresponding to the A-solution, contracts. It has two tunnels around the two branches of Γ, which expand (2). The intersection with the y,z-plane dis-

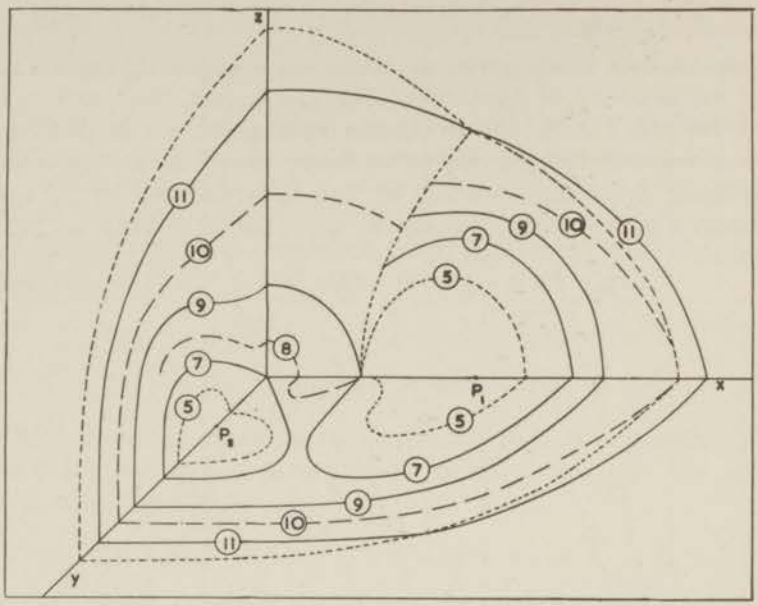

Fig.6. The resonance surfaces in h-space. Stages 5 to 11.

sociates between the axes, and bulbs are left around P_1 and P_2 on the x- and y-axis. The bulb around P_1 contracts to P_1 (4) and expands again. When it reaches Γ (5), it has a sharp edge in $(c,0,0)$ and the semi-tangent in the x,y-plane is directed along the x-axis. The bulb around P_2 contracts to P_2 (6, not in the figure) and expands. The bulbs around P_1 and P_2 associate again in the x,y-plane, and the bulb around P_2 and its symmetrical counterpart associate again in the origin. In fig.6 it is assumed that the latter association (7) takes place before the former. Whether this is true is difficult to calculate. When both associations have occurred we again have a surface with two tunnels; the tunneling part of the surface contains part of Γ, as a line of singular points. The tunnels disappear at stage 9. The semi-tangent in $(c,0,0)$ in the x,y-plane has turned over 180° from 5 to 9. From 9 on, the surface expands regularly, having, on the part of Γ between the points where the surface meets Γ from both sides in the x,z-plane, a line of singular points. In stage 10 the surface reaches the intersection of the x-axis with Ω. By 11 it reaches the point Z (the meeting points with Γ „from both sides" and the intersection with Ω at the same frequency), at 12, the intersection of the y-axis with Ω and in 13 the intersection of the z-axis with Ω (12 and 13 are not in the figure). Up to 10 we have only the resonance condition in solution A, from 10 to 13

Table I

Stage	ε	corresponding point in fig.4	h_1 in fig.4
1	0		
3	$\sqrt{(\gamma_1+\gamma_3)(\gamma_1-\gamma_2)}$	T	0
4	$\sqrt{(\gamma_2+\gamma_3)(\gamma_2-\gamma_3)}$	P_1	$\sqrt{(\gamma_1+\gamma_2)(\gamma_1-\gamma_3)}$
5	$\sqrt{2\gamma_2(\gamma_2-\gamma_3)}$	V	c
6	$\sqrt{(\gamma_1+\gamma_3)(\gamma_1-\gamma_3)}$	P_2 *)	$\sqrt{(\gamma_1+\gamma_3)(\gamma_2-\gamma_3)}$ *)
7	$\sqrt{(\gamma_1+\gamma_2)(\gamma_1-\gamma_3)}$	S	0
9	$\sqrt{2(2\gamma_1^2-\gamma_2^2-\gamma_2\gamma_3)}$	W	c
10	$\sqrt{2\gamma_2(\gamma_2+\gamma_3)}$	Q	
11	$2\gamma_2$		
12	$\sqrt{2\gamma_1(\gamma_1+\gamma_3)}$		
13	$\sqrt{2\gamma_1(\gamma_1+\gamma_2)}$		

*) these refer to h_2 instead of h_1.

the resonance condition partly in A, partly in D, both being continuously connected. From 13 on the surface expands regularly.

4. *Discussion*

The calculations of sec.3 were originally set up to obtain an interpretation of the experimental results described in Chapter III. As will be seen in Chapter IV only stage 2 of fig.5 applies to these results. As the calculations, however, led to equations for arbitrary frequency, we discussed these more or less thoroughly in sec.3. Thus a picture is obtained of the resonace surfaces in field space to be expected when frequencies are used which are greater than the one used in our experiments.

In figures 2, 4, 5, 6 we choose values of the γ_k with rather large differences $\Delta\gamma_k$ (approximately $\gamma_1:\gamma_2:\gamma_3 = 7:6:4$), so that the features would show up clearly. When $\Delta\gamma \ll \gamma$ (as is the case in copper chloride), $(c,0,0)$, P_1 and P_2, which have coordinates of the order $\sqrt{\gamma\Delta\gamma}$, lie very close to the origin compared with Ω, whose distance to the origin is $\approx 2\gamma$. The most intricate features of the behaviour of the resonance surfaces take place around

these points. At temperature zero these features should be present in the theory of YOSIDA. Due to the approximation which is made in YOSIDA's theory, however, some of these features may appear in some degenerate form. E.g. the hyperbolic branch in fig.4 in the region $c < h_1 < \gamma_1 + \gamma_2$ is degenerated into a horizontal line (cf. eq.(20)):

$$(\omega/\gamma)^2 = 2A(K_2 - K_1).$$

When $\Delta\gamma \ll \gamma$ the bulbs around P_1 and P_2 become very elongated and degenerate, in YOSIDA's case, to hyperboloid-like surfaces which at stage 6 and 4 degenerate to the axes and reappear as part of ellipsoid-like surfaces.

It may be shown that the resonance conditions (18) and the analogue of (32), $\Delta = 0$, in the x,y-plane are, as they should be, identical when we take (cf. Sec. A. 10):

$$\mu_1 = \mu_2 = \mu_3 = \mu, \qquad 2AK_1 = c^2/\mu^2, \qquad 2AK_2 = b^2/\mu^2, \qquad \alpha = 1.$$

Finally we want to mention the results of NAKAMURA[21], who calculated resonance frequencies on the basis of the spin wave theory. They are limited, however, to low temperatures as well as to small field values. As far as discrepancies occur with the classical theory, NAKAMURA is inclined to describe these to the heavy approximations made in the spin wave theory rather than to possible shortcomings of the classical theory. For these reasons we will not consider these results.

Chapter II

EXPERIMENTAL EQUIPMENT AND METHOD OF MEASUREMENT

1. *Introduction*

The experimental task in this investigation was to measure absorption of electromagnetic waves in a substance at low temperatures as a function of an external magnetic field. The measurements were performed at wavelengths of 3 and 7 cm.

Electromagnetic waves in these wavelength regions are excited by monochromatic oscillators, usually reflex klystrons. The waves are propagated in coaxial lines or wave guides. A convenient device to measure small absorptions is the resonant cavity which may be considered as a length of closed transmission line (coaxial or guide). The electromagnetic wave, reflected at each end, travels up and down, and thus the effect of the absorption by a substance in the cavity, is multiplied.

The method we used is the transmission loss method. The cavity is coupled to two transmission lines, one connected to the oscillator, the other connected to a detector. Only when the cavity is resonant with the applied frequency an appreciable part of the high frequency input energy is transmitted to the output. A change in the output is a direct measure of the change in the absorption in the cavity, when the input is kept constant.

Low temperatures of the sample were obtained by cooling the cavity. The external field was provided by an electromagnet.

Experiments have been carried out with microwaves of about 3 cm and 7 cm wavelength. For each wavelength a completely separate experimental set up was needed, only the electromagnet and the vacuum pump being common to each series of experiments.

The experimental set up for the 3 cm region was, except for some small alterations, the same one as used by BIJL[26] for his paramagnetic resonance measurements. But, for completeness, we will give a brief description of it again.

2. *The experimental equipment.*

A schematic diagram of the experimental arrangement is shown in fig. 1. The microwave equipments for both wavelengths, consis-

ting of klystron, cavity and detector coupled in series by transmission lines, will be discussed in some detail in the following sections.

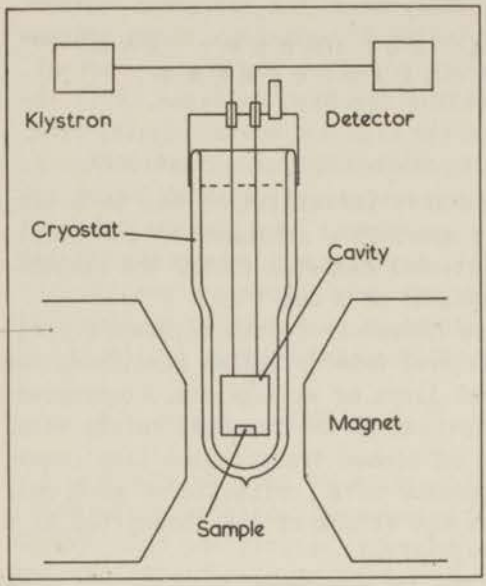

Fig.1. The experimental arrangement

The cavity was mounted in a cryostat and the low temperatures were obtained with a bath of liquid nitrogen, hydrogen or helium. The temperature was regulated and determined through the vapour pressure of the coolant. The cavity could be evacuated through a pumping line (not in the figure) connected with a rotary pump, in order to prevent condensations in the cavity. In the later experiments we let helium gas into the cavity at a few millimeters pressure in order to establish a better heat contact between the sample and the walls of the cavity.

The magnet used could produce fields up to about 15000 Ø at the required distance of the pole pieces. It could be rotated so that the orientation of the field with respect to the cryostat apparatus was adjustable. Its position was read on a circular scale.

3. *Oscillators*

The 3 cm oscillator used was a reflex klystron, British type *CV* 129. The normal ratings of this tube are:

Heater current	1.4 *A*;	heater voltage 4 *V*.
Resonantor voltage	1.6 *kV*	with respect to cathode.
Reflector voltage	-300 to -550 *V*	" " " "
Grid voltage	-5 to -100 *V*	" " " "
High frequency output	100 *mW*.	
Frequency	9550 - 9200 *MHz*.	

Since the resonator is connected to the wave guide, it is convenient to earth the resonator and the cathode voltage be-

comes -1.6 *kV*. The tube was heated by two 2 *V* accumulators and batteries supplied the high voltages.

The frequency could be adjusted roughly to the resonance frequency of the cavity by a screw which deforms the resonator and, more accurately, by small variations of the reflector voltage.

In fig.2 the connections to the klystron are shown schematically. *H* are the accumulators providing the heater current. *V* are a set of batteries providing the high voltages. *W* is the waveguide connected to the klystron with a piece of coaxial line. The output of the tube may be regulated by the potentiometer *A*. B_1 and B_2, two potentiometers in parallel, are used to adjust the reflector voltage. Keeping the adjustment of B_2 constant, small changes in the reflector voltage originating through adjustment of B_1 are measured by the microammeter *P*. Thus a qualitative measurement of changes in the frequency is possible. In case this is of no interest the connector *S* is opened.

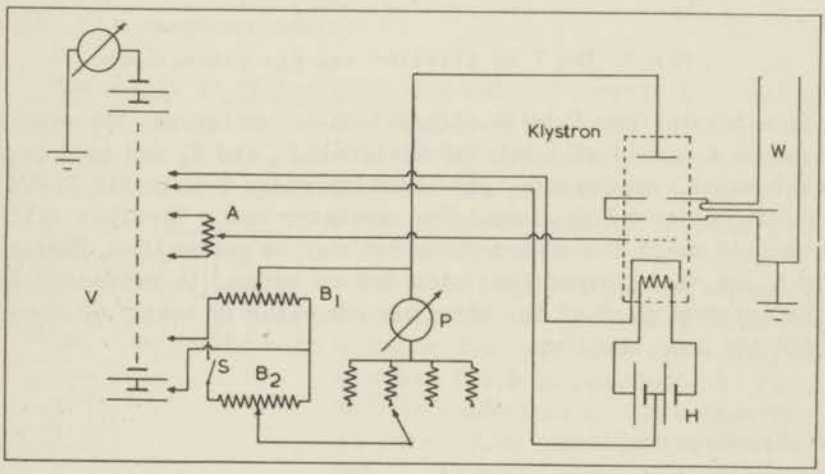

Fig.2. The 3 cm klystron and its connections

The 7 cm oscillator used was a non-reflex klystron kindly put at our disposal by PHILIPS N.V., Eindhoven. The electronic part is shown schematically in fig.3, with its connections.

The resonator is partly inside, partly outside the vacuum tube. It has two apartments *S*, inside the vacuum tube, through which the electron beam is directed. In the first the beam is bunched and in the second the bunches deliver energy to the resonator. The heater voltage, $V_F = 6.3$ *V*, and the resonator voltage, $V_S \approx 375$ *V*, were taken from a power supply. The grid voltages $V_{B1} = -100$ *V* and $V_{B2} = +105$ *V* were obtained with batteries and

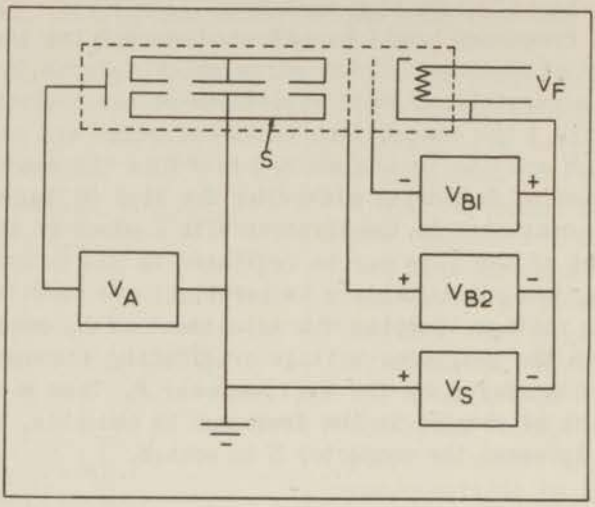

Fig.3. The 7 cm klystron and its connections

the anode voltage V_A with nickel-iron-accumulators. The electron beam is focussed with help of the grids B_1 and B_2 and by a permanent magnet around the tube which provides a magnetic field in the direction of the beam. The resonator has a flexible wall by means of which the output frequency may be controlled. Energy up to a few watts, over the 7.4 - 7.6 cm range, is extracted from the external part of the klystron resonator by means of coaxial line and loop coupling.

4. *Resonant cavities*

A resonant cavity may be considered to be a section of low loss transmission line of such a construction that standing waves may be excited in it. A given cavity may oscillate in several modes, each mode having a characteristic frequency, a characteristic electromagnetic field pattern and loss factor. The cavity may be coupled by loops or probes with the transmission lines to the oscillator and the detector. Due to losses in the walls, in the contents of the cavity, and in the coupling devices, the electromagnetic oscillation is damped. A measure of the damping is the quality factor Q, of the cavity, defined by

$$Q = 2\pi \frac{\textit{energy stored}}{\textit{energy dissipated per cycle}} \quad \text{when the cavity is in resonance.} \tag{1}$$

It may be shown that the absorption A in the cavity is inversely proportional to the quality factor: $A \sim 1/Q$ (Q>>1). When the absorption in the cavity is changed, we have for the change in absorption

$$\delta A = A - A_o = \alpha(1/Q - 1/Q_o) \qquad (2)$$

where α is some proportionality factor, and Q_o and Q are the quality factors of the cavity before and after a change of the absorption.

In general, a change in the absorption by the material in the cavity, which is connected with the imaginary part of the complex susceptibility of the material, will be accompanied by a change in the real part, which is dispersion. This is detected by a change in the resonance frequency.

5. *The 3 cm resonance cavity*

The cavity is cylindrical. The mode of oscillation used is the H_{111}-mode, the mode with the natural lowest frequency. Fig.4 shows the field pattern schematically. As we are interested in magnetic rather than electric transitions in our samples, a suitable position for the sample is at the bottom of the cavity where the magnetic field is most dense and the electric field the weakest. The H_{111}-mode is degenerate in the mathematical case of an exactly cylindrical cavity since the plane of symmetry of the mode of oscillation is not fixed apriori. In practice the degeneracy will be removed by the coupling deviced and the sample, but the difference of the resonance frequencies will generally be much smaller than the width of the cavity resonance curve and thus not detectable. In one experimental setting, however, we found two resonance frequencies different enough to correspond to two completely separated cavity resonance curves. In general it is difficult to predict the actual direction of the oscillating field exactly, but it may be determined afterwards from the paramagnetic measurements (cf.sec.13).

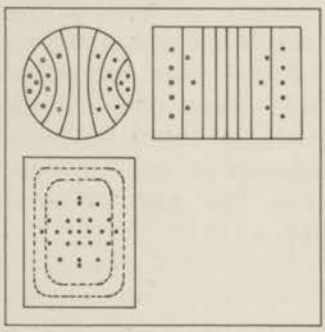

Fig.4. The field pattern of the H_{111}-mode in three perpendicular planes through the centre of the cavity.
——— electric field
- - - - - magnetic field

For the H_{111}-mode, the relation between the dimensions of the cavity and the resonance frequency is

$$f = (v/2)\left[(1.84/a)^2 + 1/l^2\right]^{1/2} \qquad (3)$$

where f = resonance frequency (in sec^{-1}),
v = velocity of light in the medium filling the cavity (in $cm.sec^{-1}$),
a = radius of the cavity (in cm),
l = length of the cavity (in cm).

a was chosen to be 1.05 cm. From (3), with f = 9400 MHz, v = velocity of light in vacuum, we obtain l = 3.28 cm. In reality l was chosen somewhat shorter, as the presence of the sample reduces the resonance frequency.

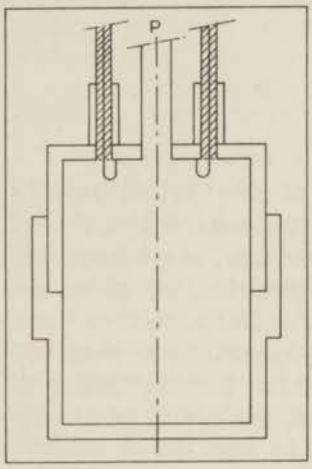

Fig. 5. The 3 cm cavity

Fig. 5 shows the construction of the cavity with the coupling devices. The upper and lower part were soldered together with Wood's metal. The slit between the two parts is in the middle of the cavity where there are no appreciable vertical currents (as may be derived from the field pattern), thus, practically, it will not affect the quality factor. The cavity can be evacuated through the pumping line P. The input and output coupling are small loops (H-coupling) formed by soldering the inner conductor to the outer conductor of the Pyrotenax cables which form the ends of both transmission lines.

6. *The 7 cm resonance cavity*

A cylindrical cavity cannot be used at 7 cm since it would be too large for mounting in a cryostat. For this reason a coaxial cavity is used. This is a cylinder with a stub extending from one end for about $\lambda/4$ (λ = wavelength). The electric fields have a node at the bottom and an antinode near the end of the stub; for the magnetic fields the case is reversed. Thus the sample to be investigated is placed at the bottom where, again, we have a dense high frequency magnetic field and practically no electric field.

Due to end corrections, the length of the stub is not exact-

ly $\lambda/4$. In the case where the end of the cavity opposite to the stub is sufficiently far away to have no effect, the length of the stub l is given by

$$Z_o \tan(2\pi/\lambda)\, l = 1/\omega C_o. \qquad (4)$$

Z_o is the characteristic impendance of the coaxial line

$$Z_o = 138\ \log_{10}(a/b)\ ohms$$

where a is the radius of the cavity and b that of the stub; C_o is the free space capacitance of a circular disk with the same cross section as the stub.

It was an advantage, however, in connection with the coupling problem, to have the upper end of the stub not too far away from the top of the cavity, thus increasing the effective value of C_o. l was estimated with help of (4), for an increased value of C_o and the correct length was experimentally adjusted. The stnb was ground off untill the cavity was adjusted to the oscillator frequency.

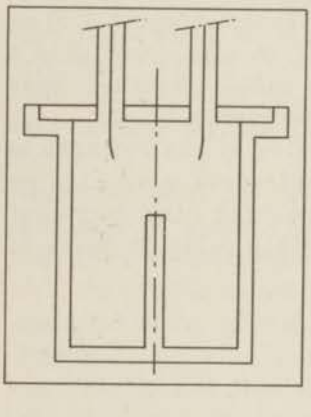

Fig.6. The 7 cm cavity

In view of the dimensions of the available cryostat, a was limited to be 1,00 *cm* and b was chosen to be 0.15 *cm*. After adjustment, the stub had a length of 1.59 *cm*.

The 7 cm cavity is shown in fig.6. The lower part is soldered to the top with Wood's metal. The input and output coupling are provided by the inner conductors of the transmission lines which extend into the cavity through the top cover. The coupling is to the electric field in the region between the end of the stub and the top.

7. *The transmission lines*

3 cm set. In the 3 cm region wave guides are the most desirable form of transmission lines. A length of British wave guide was used to connect the oscillator to the cryostat apparatus. A variable attenuator was required in the guide to adjust power reaching the cavity and to diminish undesirable resonance phenomena. The guide was coupled to the klystron by a coaxial line as

shown in fig.2. Waveguides were impracticable inside the cryostat because of their size and because the heat conduction would be unduly large unless the waveguides were of a special construction, e.g. guides consisting of glass, silvered on the inside. Therefore, coaxial lines were constructed of thin walled brass tubes with paraffine wax as the insulator, the combination having a sufficiently small rate of heat conduction. The coaxial leads were connected to the cavity and to the waveguides with pieces of Pyrotenax cable. The losses in these leads were very high at room temperature but decreased sufficiently at lower temperatures to make measurements possible.

7 cm set. Waveguide for 7 cm was not available and coaxial lines were used which had an attenuation low enough to be practicable. Standard flexible 50 *ohm* cable was used outside the cryostat. The oscillator had enough power to permit the use of rather long lengths of cable. The attenuation introduced in this way diminished the resonant effects. To reduce the heat loss by conduction, the coaxial lines inside the cryostat were constructed of German silver tubing. The inner diameter of the outer conductor was 7.00 *mm* and the outer diameter of the inner conductor 3.00 *mm*. This yielded a characteristic impedance of 55 *ohms*, providing a satisfactory match to the 50 *ohm* flexible cable. The inner conductor was supported by rings of polystyrene placed in such a way that reflections at one ring would be canceled by the reflections at another ring. Since these coaxial leads were used also as pumping lines, small sections of the supporting rings were cut away. The leads were connected to the flexible cable by means of vacuumtight feed-throughs.

8. *Detectors*

The detector consisted of a 1*N*21 crystal connected to a sensitive galvanometer. The characteristic of this rectifier is approximately „square law", i.e. the rectified current is approximately proportional to the square of the high frequency input voltage. Since we were unable to calibrate the crystal rectifier frequently we assumed the square law to hold in our calculations. This is only approximately correct. Thus our calculations of the rate of change of absorption are only qualitative.

In the 3 cm set, the crystal rectifier was placed across the end of a piece of waveguide and leads were brought out to the galvanometer.

For the 7 cm set, the crystal was mounted in a unit which also contained a wavemeter.

9. *The measurement of frequency.*

Frequencies were measured with adjustable cavity wavemeters. At 3 cm we used a cylindrical cavity in one end of which there was a variable plunger. The wavemeter was coupled to the waveguide with a piece of Pyrotenax cable and calibrated against a Test Set. For 7 cm, the wavemeter consisted of a surplus (U.S.) adjustable coaxial resonator. In both cases the accuracy of the frequency measurements was estimated to be roughly 0.2%.

10. *Method of measuring the absorption*

The change in the absorption of the crystal placed in the cavity was measured by the change in the galvanometer deflection. It may be shown that the power reaching the detector is proportional to Q^2 when the cavity is in resonance. For this to be true the direct coupling between the coupling loops or probes must be negligable. Then, assuming the rectified current proportional to the power input to the detector, the change of absorption, using (2), is

$$\delta A = \alpha(1/Q - 1/Q_0) = \alpha'(Q_0/Q - 1) = \alpha'[(\delta_0/\delta)^{1/2} - 1] \qquad (5)$$

where δ_0 and δ are the galvanometer deflections before and after a change of absorption (resonance being maintained throughout) and α' is a proportionality factor.

In all our measurements the absorption with certain external magnetic field is compared with the absorption for zero field. We computed $(\delta_0/\delta)^{1/2} - 1$, where δ_0 is the galvanometer deflection in zero field, and plotted this versus H. It must be remembered that (5) gives the change in absorption in arbitrary units since α' is unknown. For our purposes, however, this is not important since we are mainly interested in the field values corresponding to maximum absorption. As far as we may draw conclusions about the intensity of the absorption, they must remain qualitative.

The course of a measurement at 3 cm was as follows. After the cavity containing the sample had been evacuated and the cryostat filled with the coolant, the klystron was tuned to the resonant frequency of the cavity by means of the mechanical frequency adjustment. The magnet was placed in the desired direction and the galvanometer deflection observed for a series of field values. For each value of the magnetic field, the klystron was tuned to resonance with the cavity by adjusting the reflector voltage for a maximum galvanometer deflection. This was necessary in order to

avoid the effect of the detuning resulting from the crystal dispersion (cf. sec. 4) and from frequency drift of the klystron.

The galvanometer deflection for zero field, δ_0, was determined from time to time and the value belonging to a particular measurement of δ was found by interpolation. Sometimes δ_0 drifted considerably. This was ascribed both to a change in the attenuation of the coaxial leads in the cryostat, due to change in the temperature of the lines when the level of the liquid fell and to changes in the quality factor of the cavity resulting from condensations in the cavity. The galvanometer zero might drift slowly due to changing thermocouples in the galvanometer circuits. These were eliminated as much as possible by observing the zero with the klystron out of oscillation.

When dispersion effects were to be measured, the change in reflector voltage at which maximum galvanometer deflection occurred was used as a measure of the frequency, as described in sec. 3.

In the 7 cm case the course of a measurement was practically the same. Here the klystron was tuned only by a mechanical adjustment of the klystron resonator. Changes in this adjustment, and thus in the frequency, were read on a dial fixed to the adjusting screw.

11. *The copper chloride crystals*

$CuCl_2.2H_2O$ crystals have orthorhombic symmetry and may be grown in long needles. The axis of these needles is the *c*-axis. The cross section perpendicular to the *c*-axis is a rhomb in which the shortest diagonal is the *a*-axis and the larger the *b*-axis. Crystals were ground to have a flat side parallel to two axes. When put on this side on the bottom of the cavity, one crystal plane was horizontal and the external magnetic field, which could be orientated in a horizontal plane, was confined to directions in this particular crystal plane. In the following we will refer to the *a, b*- or *a, c*-crystals, cases etc. as to the crystals, cases etc. in which the *a, b*-plane or *a, c*-plane was horizontal, and thus the external field confined to this plane. Measurements were carried out on one *a, b*-crystal and two *a, c*-crystals.

Crystals of copper chloride are not very stable. They deliquesce with ease. For protection, the *a, b*-crystal was placed in a small quartz casket; VAN DEN HANDEL, GIJSMAN and POULIS[11] had prepared it in this way for their susceptibility measurements. We tried to protect the first of the *a, c*-crystals with a thin layer

of celluloid. This proved unsuccesful. After a few measurements the crystal had completely disintegrated. The second a, c-crystal was placed in a small polythene casket sealed off with paraffine wax, with more success.

The growing of single copper chloride crystals is a difficult operation. We are much indebted to Dr.N.J.Poulis for providing our samples.

12. *The orientation of the crystal with respect to the external field*

The orientation of the crystal was determined by observing the orientation of the crystal with respect to the cavity, when it was open, and the orientation of the cavity with respect to the magnet when the cavity was fixed to the cryostat apparatus. Since the crystals were very small, perhaps 2 or 3 mm on a side, the determination of the crystal orientation with respect to the cavity was rather difficult. The accuracy of the determination of the final orientation was estimated to be about one degree. The dependence of the resonance field on the field orientation was determined in the paramagnetic measurements of the anisotropy of the g-value. Because this field value is a maximum or a minimum along the axes, the orientation of the crystal could be confirmed by these measurements.

13. *The orientation of the high frequency oscillating field in the cavity.*

The orientation of the high frequency field is of importance in the discussion of polarization effects. For the 7 cm cavity, the oscillating magnetic flux at the bottom is concentric with the axis of symmetry. Thus, in the crystal, the field is effectively perpendicular to the radius on which the crystal is placed. In the 3 cm cavity the mode of oscillation is degenerate (cf. sec. 5) and the direction will be determined by the coupling loops and the shape of the crystal. The exact orientation will be difficult to predict. It may be determined, however, from the paramagnetic absorption measurements. The resonance absorption depends on the angle between the direction of the external field and that of the oscillating field. It is a minimum when this angle is zero. In other words, the direction of the oscillating field is the direction of the external field when the paramagnetic resonance absorption is a minimum.

In the 3 cm measurements on the a,b-crystal we found two distinct resonant responses not far apart in frequency. The mode degeneracy had obviously been removed. The directions of the oscillating field belonging to the two modes, appeared to be perpendicular. This fact, which was not premeditated, could be used to obtain more polarization data from one experimental mounting.

Chapter III

EXPERIMENTAL RESULTS

Introduction

Experiments have been carried out on two single crystals of copper chloride $CuCl_2.2H_2O$), one an a,b-crystal and the other an a,c-crystal. 3 cm measurements ($\nu = 9.4_1.10^3$ MHz) have been made on both these crystals, 7 cm measurements ($\nu = 3.9_8.10^3$ MHz) only on the a,c-crystal. 3 cm measurements on another a,c-crystal had to be disqualified because this crystal had disintegrated to a far extent; the latter measurements could be interpreted satisfactorily, in a qualitative way, by assuming that the crystal had obtained an oblique orientation with respect to the apparatus, but they are hardly of any value and, hence, will not be considered.

It was in the 3 cm-a,b-measurements that two modes of oscillation of the cavity occurred (cf. II sec. 5, 12).

The absorptions have been measured as a function of the external field for different orientations of this field with respect to the crystal axes and at different temperatures. By "absorption" we mean the quantity $A = \sqrt{\delta_0/\delta} - 1$. As shown in Ch. II, sec. 10, this is closely related to the true absorption in the crystal but is not a very reliable quantity when accurate quantitative comparisons between absorptions are desired.

Measurements have been made above and below the Néel temperature. The former correspond to paramagnetic resonance and were carried out in liquid nitrogen or liquid hydrogen. The latter correspond to antiferromagnetic resonance and were carried out in liquid helium. the paramagnetic absorption measurements are of secondary importance here since they were carried out chiefly as control experiments in the determinations of the orientations of the crystal axes and the directions of the high frequency fields. However, as a by-product, g-values were obtained.

To facilitate comparing the results of the paramagnetic with the results of the antiferromagnetic experiments, and the latter with each other, it was desirable to have the circumstances of the individual measurements as nearly alike as possible. Therefore, once the cryostat apparatus was mounted with a sample in it, it was left unchanged whenever possible until all the measurements on the sample were finished.

As to the accuracy of the measurements, the main origin of the uncertainty in the results appears to be the calibration of the external magnetic field and the determination of the orientation of the crystal axes. As no very careful attention was paid to the calibration of the magnet, there will be an uncertainty in the absolute values of the fields of 1 or 2%.

A. The paramagnetic resonance measurements

Fig.1 shows a typical paramagnetic absorption curve obtained by plotting the absorption A versus the external field H. From such absorption curves we obtain the resonance fields (the central H-values of the absorption lines) and the maximum absorption.

When the resonance fields are plotted versus the orientation of the external field, sinusoidal curves are obtained which exhibit the anisotropy of the g-factor. A comparison between the measurements in liquid nitrogen and those in liquid hydrogen did not reveal any temperature dependence.

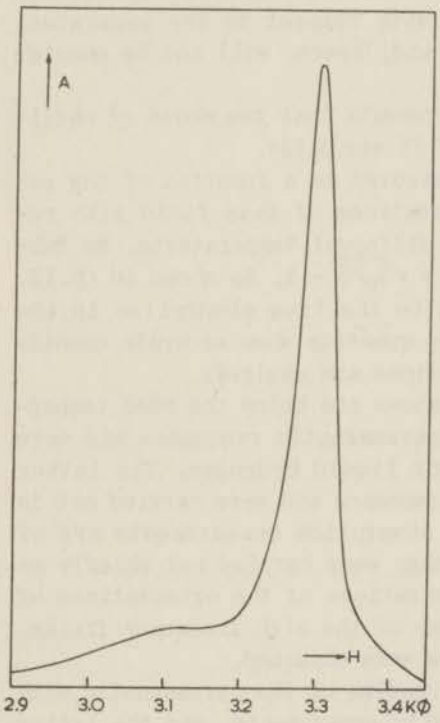

Fig.1. Absorption A versus magnetic field H at 3 cm. $\mathbf{H} \parallel b$-axis.
T = 14.2 °K. Mode II.

The orientations of the external fields at which extreme values of the resonance fields occur, coincide, within the limits of accuracy, with the directions of the crystal axes as determined when the crystals were mounted into the apparatus. From these extreme values of the resonance fields, the g-values along the axes are derived with the aid of

$$h\nu = g\beta H \qquad (1)$$

(h is Planck's constant, ν is the frequency, β the Bohr magneton and H the resonance field). The g-values obtained differ about 1 or 2% from those given by Itoh[27], but there is no reason to speak of a disagreement,

as our results are affected by an uncertainty of this amount in the absolute values of the resonance fields (cf. introduction).

If the maximum values of the absorptions, found from the absorption curves, are plotted versus the orientation of the external field, the minima of the resulting curves yield the orientation for which the external field is parallel to the oscillating field in the cavity (cf. Ch. II, sec. 13). It appeared that in the 3 cm-a, b-case the oscillating field made an angle of 15° with the a-axis in one mode of oscillation (mode I), and -75° with the a-axis in the other mode (mode II); in the 7 cm-a, c-case the oscillating field was directed practically along the a-axis. These data are of importance when polarization effects are discussed. In the 3 cm-a, c-case no paramagnetic measurements were made.

We have not paid much attention to the line widths. The line widths, defined as the field width of the line where "the absorption" A is half the maximum absorption, do not show any definite dependence upon temperature or orientation and are roughly spread over the range 60 to 80 Ø. Due to the not very reliable relation between A and the real absorption a considerable spread might be expected.

Fig. 1 shows an example of an additional absorption which has been observed to occur occasionally on the low field side of the main absorption peak in the case of the 3 cm, a, b-crystal, particularly in the later measurements. It must probably be ascribed to partial disintegration of the crystal. The copper ions which are no longer contained in the regular crystal lattice will, on the average, give an absorption at a field somewhere between the resonance fields along the three axes. This agrees with the observations.

Approximate dispersion curves were obtained, in a few cases, by noting the change in the resonant frequency of the cavity (cf. Ch. II, sec. 3, 4). The form of these curves was, as expected, a dip just before and a peak just after the absorption line.

B. The 3 cm antiferromagnetic resonance measurements

1. *Introduction.* 3 cm absorption measurements below the Néel point were carried out at a number of temperatures between 1.2 and 4.2°K. The properties of the resulting absorption diagrams may be described briefly as follows:

At the lowest temperatures, two rather narrow absorption lines are found when **H** is directed along the x-axis. As **H** is rotated towards the y-axis, these lines broaden, approach one another, coalesce and then disappear rapidly. This behaviour is

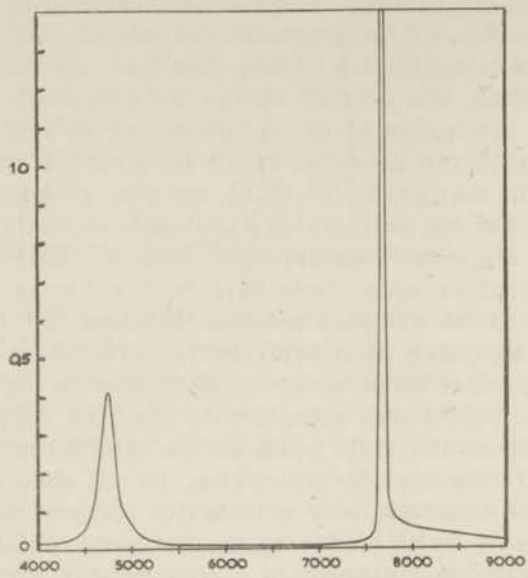

Fig. 2. Absorption A versus magnetic field H (in Ø) at 3 cm. $\mathbf{H} \parallel$ a,b-plane. Angle θ between $\mathbf{H}$ and a-axis = 1°. $T = 3.29$°K.

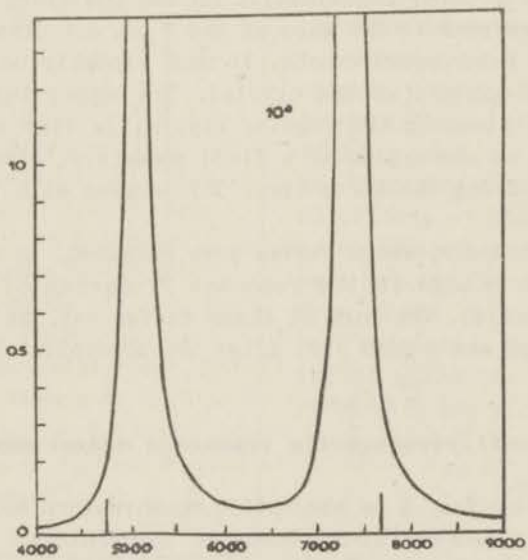

Fig. 3. Absorption A versus magnetic field H (in Ø) at 3 cm. $\mathbf{H} \parallel$ a,b-plane. Angle θ between $\mathbf{H}$ and a-axis = 10°. $T = 3.29$°K.

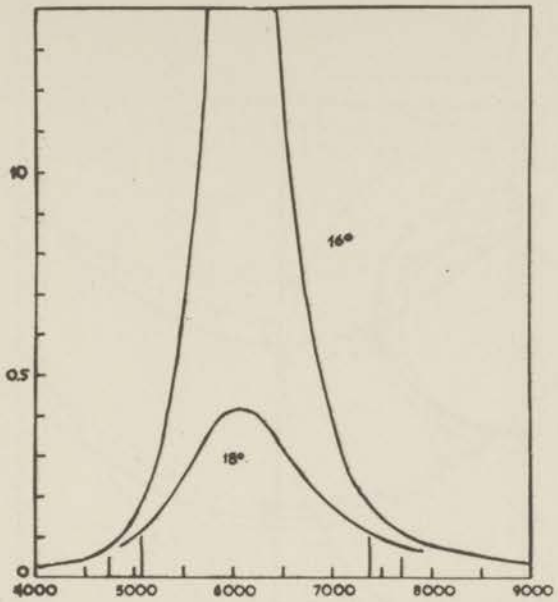

Fig. 4. Absorption A versus magnetic field H (in Ø) at 3 cm. $\mathbf{H}_{\parallel}$ a,b-plane. Angle Θ between $\mathbf{H}$ and a-axis = 16° and 18°. T = 3.29°K.

illustrated in figures 2, 3, 4. On the other hand, as $\mathbf{H}$ is rotated from the x-axis towards the z-axis, both these lines shift to higher field values. This goes on until they have reached the strongest field obtainable with the magnet used in the investigation. Meanwhile there is a gradual broadening of the lines.

When the temperature is raised, both these lines broaden and move away one from another. This occurs up to about 4.0°K. Above this temperature the higher field line, for $\mathbf{H}$ parallel to the x-axis, becomes asymmetric and finally degenerates into a case of „threshold absorption". That is, when H is increased, the absorption increases rapidly in a small interval of H and remains roughly constant for larger H-values. When $\mathbf{H}$ is rotated towards the y-axis this absorption returns again to a more normal line shape.

In the following sections we shall give a more detailed analysis of these observations.

2. *Line positions.* When the absorption lines have a sufficiently symmetrical shape we may define the central H-value of the line as the line position. When, at the higher temperatures, the absorption curves show pronounced asymmetry, we take for the

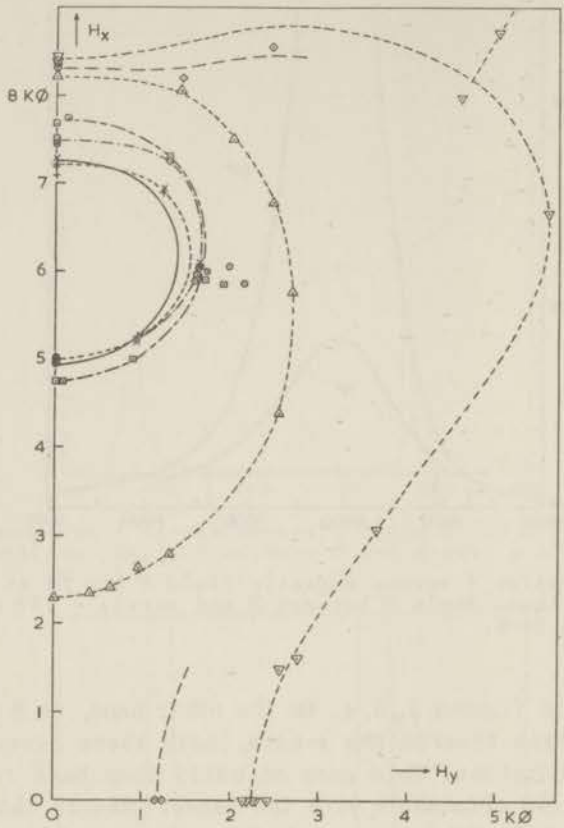

Fig.5. Line positions in the X,Y-plane, 3 cm.

▽ T = 4.22°K.

◇ { T = 4.11°K. T = 4.15°K.

△ T = 3.98_3°K.

⊡ T = 3.29_5°K.

⊙ { T = 3.03_2°K. T = 3.01_8°K.

× { T = 1.43°K. T = 1.39°K.

+ { T = 1.27°K. T = 1.23_6°K.

line position the H-value corresponding to the maximum absorption. To enable us to see the behaviour of the line positions, they are plotted in H-space. Defining the X-, Y-, and Z-axes in H-space as parallel to the a-, b- and c-axis, respectively, in the crystal, we obtain line positions in the X,Y-plane from the ob-

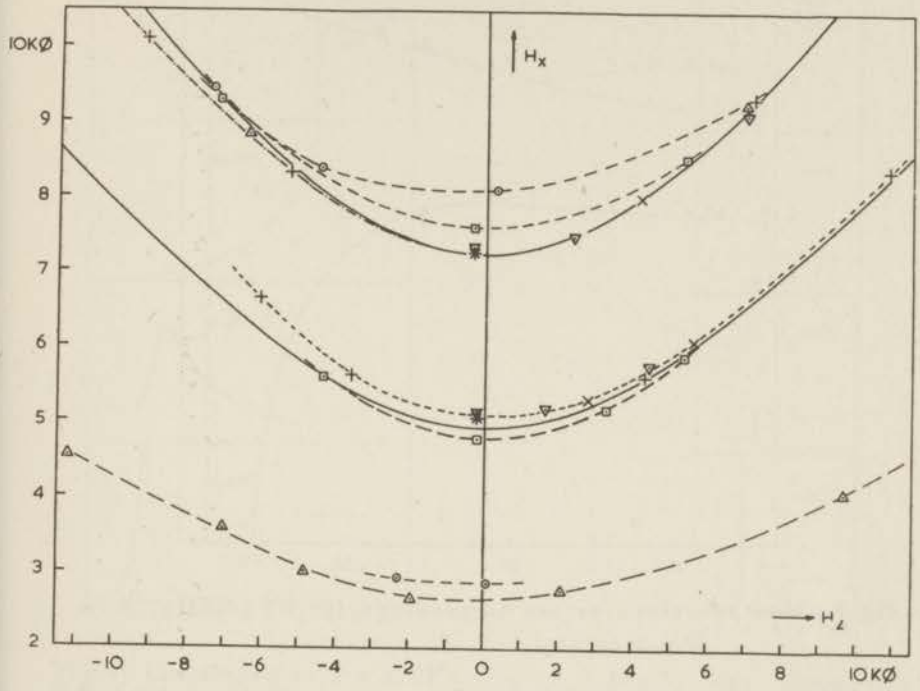

Fig. 6. Line positions in the X, Z-plane, 3 cm.

△ T = 3.88_3°K. ▽ T = 2.53_3°K.
⊙ T = 3.87_5°K. × T = 1.89_5°K.
⊡ T = 3.03_2°K. + T = 1.31_2°K.

servations on the a, b-crystal and line positions in the X, Z-plane from the observations on the a, c-crystal. The results are shown in figures 5 and 6.

We would expect these resonance curves in both cases to be symmetrical with respect to the X-axis. With the a, b-crystal (fig. 5) this symmetry has been experimentally checked at a few points. With the a, c-crystal (fig. 6) this symmetry is obtained to a reasonable degree by assuming the direction of the X-axis to differ somewhat from the direction of the X-axis as determined when the crystal was mounted in the apparatus. In plotting the points in fig. 6, we have corrected the direction of the X-axis by 2.4^0 for one experimental mounting and by 2.7^0 for another mounting. Note that in fig. 6 H_y has been given in a scale twice as large as H_x.

In the X, Y-plane, fig. 5, closed curves obtain which expand when the temperature increases. At temperatures greater than about

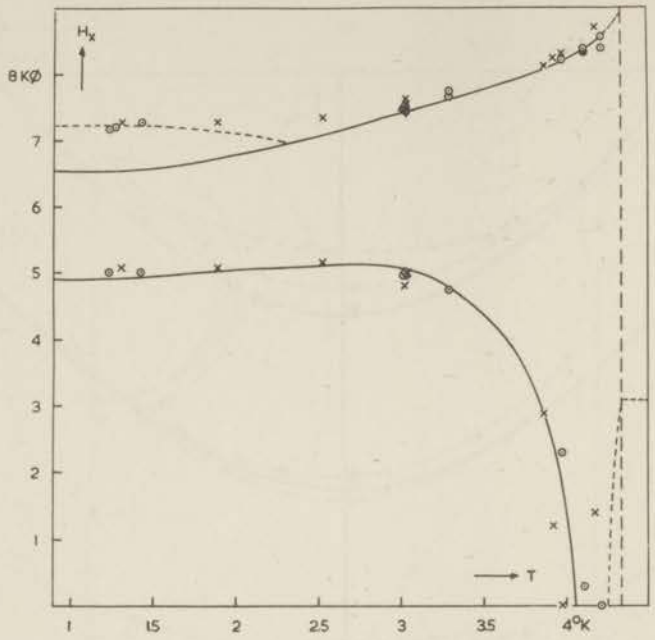

Fig.7. Line positions versus temperature for **H** ∥ *X*-axis, 3 cm.
⊙ *a*, *b*-crystal, × *a*, *c*-crystal.

$4^{\circ}K$, the absorption curves become more and more asymmetric and so the notion of „line position" becomes somewhat indefinite. This is probably the reason why the points show considerable scatter at these temperatures.

In the *X*, *Z*-plane, fig.6, we obtain two nearly hyperbolic curves which move away from another with rising temperature.

The full-drawn curves in figures 5 and 6 represent theoretical curves, to be discussed in Chapter IV.

Figure 7 shows the line positions as functions of temperature when **H** is directed along the *X*-axis. It is seen that the line positions are practically independent of temperature below about $2.5^{\circ}K$. The lines, corresponding to the lowest branch in fig.7 in the temperature range $3.92 - 4.22^{\circ}K$, have widths of the order of 2 kØ. These large line widths must be one of the reasons of the considerable scatter among the values assigned to the resonance fields in this region. An uncertainty in the temperature determination due to imperfect thermal equilibrium between the crystal and its surroundings in another probable reason for scatter. The dashed and full-drawn curves will be discussed in Ch. IV.

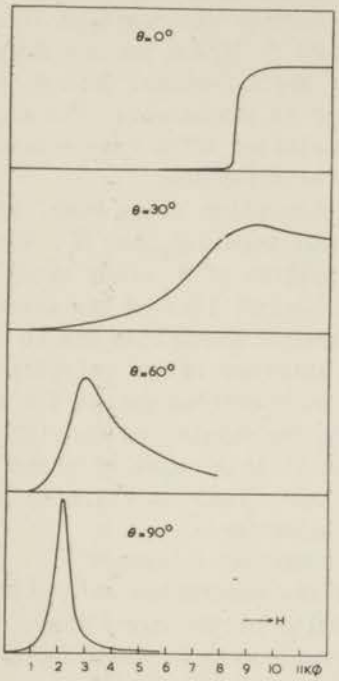

Fig.8. Lineshapes at $T = 4.22^{\circ}K$, $\mathbf{H} \parallel X,Y$-plane, 3 cm. θ = angle between $\mathbf{H}$ and the X-axis.

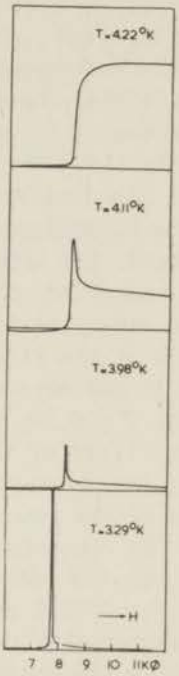

Fig.9. Line shapes at different temperatures. $\mathbf{H} \parallel X$-axis, 3 cm.

3. *Shapes of the absorption curves.* In the a,b-case we found „threshold absorption" at $4.22^{\circ}K$ when $\mathbf{H}$ was directed along the X-axis. As $\mathbf{H}$ was rotated towards the Y-axis this „threshold pattern" diminished until, for $\mathbf{H}$ parallel to the Y-axis, a normal line shape was obtained. This is illustrated in fig.8.

When $\mathbf{H}$ is kept parallel to the X-axis but the temperature is decreased to $4.13^{\circ}K$, the absorption continues to rise sharply at a certain value of H, for increasing H, but falls again immediately afterwards and remains roughly constant at a value larger than the zero field absorption. This constant absorption on the high field side of the peak degenerates into a small tail at lower temperatures. It is still seen at $3.29^{\circ}K$, but scarcely observable at lower temperatures. This behaviour is illustrated in fig.9. It was reproduced more or less with the a,c-crystal as well.

4. *Intensities of the absorption.* Figures 10 and 11 show the maximum values of the absorption observed with the a,b- and the a,c-crystal respectively. These data are qualitative at most (cf. Chapter II, sec.10).

In fig.10, the maximum absorption has been plotted against an angle η. η is defined as the angle between the positive X-axis and the line joining the point $H_x = 6200$ Ø, $H_y = 0$, on the X-axis to the corresponding line position in the X,Y-plane. This method of plotting the data is purely a matter of convenience. The angle η is one of the most easily defined variables which vary monotonically along the resonance curves in the X,Y-plane.

Fig.10 gives the height of the absorption ridge when, in a three dimensional picture, A is plotted versus H_x and H_y. When, however, the line representing the direction of H, along which we are measuring, does not intersect the central line of the absorption ridge, we yet may observe a maximum of absorption due to the width of the ridge. The maximum then obtained is not relevant to fig.10 and corresponding points have been omitted except for the point $T = 3.29_5{}^{\circ}K$, $\eta = 99^{\circ}$, which may be considered to yield a lower limit of the maximum absorption at this value of η and T. This consideration explains, also, the points in fig.5 to one side of the resonance curves at low temperatures.

In connection with fig.10 we want further to remark:

a. The rather steep increase of the absorption at $\eta \approx 160^{\circ}$ for $T = 4.22^{\circ}K$ and the abrupt termination of the curve there is connected with the shape of the resonance curve in the X,Y-plane. at this temperature.

b. Points obtained at $T = 4.22^{\circ}K$ in mode II have been omitted. They give absorption values much lower than those in mode I for all η and do not show any marked dependence upon η.

c. At lower temperatures, points in mode II are obtained only for $\eta = 0^{\circ}$ and 180° (corresponding to the two resonance lines along the X-axis).

From fig.10 we obtain the following qualitative results:

a. In general, the absorption increases with decreasing absorption. A remarkable exception is the absorption for $T = 1.33^{\circ}K$ at $\eta = 0$ which is lower than those for $\eta = 0$ at the next higher temperatures.

b. Except for the highest temperatures, the absorption as a function of η shows a maximum for values of η in the range 80 to 100°.

c. At the lower temperatures, the absorptions in mode II are considerably lower, for $\eta = 0^{\circ}$, and considerably higher, for $\eta = 180^{\circ}$, than those in mode I. At the highest temperature the absorptions in mode II are lower than those in mode I for all η.

Fig.11 shows the maximum values of the absorption obtained with the a,c-crystal. Here, we chose, as independent variable along the resonance curves, the angle θ between the X-axis and the external field. For the rest, fig.11 is self explanatory.

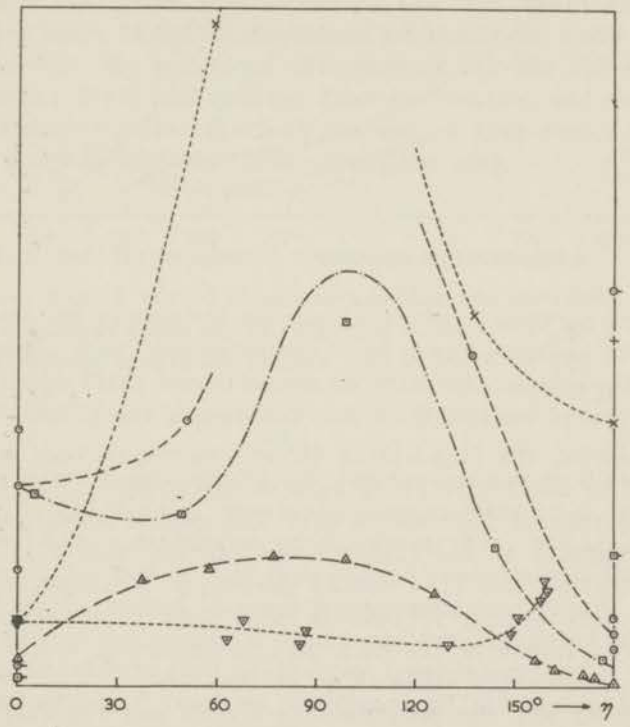

Fig.10. Maximum absorptions versus η in the 3 cm-a, b-case.

▽ T = 4.22°K, mode I
△ T = 3.98°K, mode I
⊡ T = 3.29_5°K, mode I
⊡ T = 3.29_5°K, mode II
⊙ { T = 3.03_2°K, T = 3.01_8°K } mode I
⊙ { T = 3.03_2°K, T = 3.01_8°K } mode II
\+ { T = 1.32_8°K, T = 1.27°K } mode I
× { T = 1.43°K, T = 1.39°K } mode I

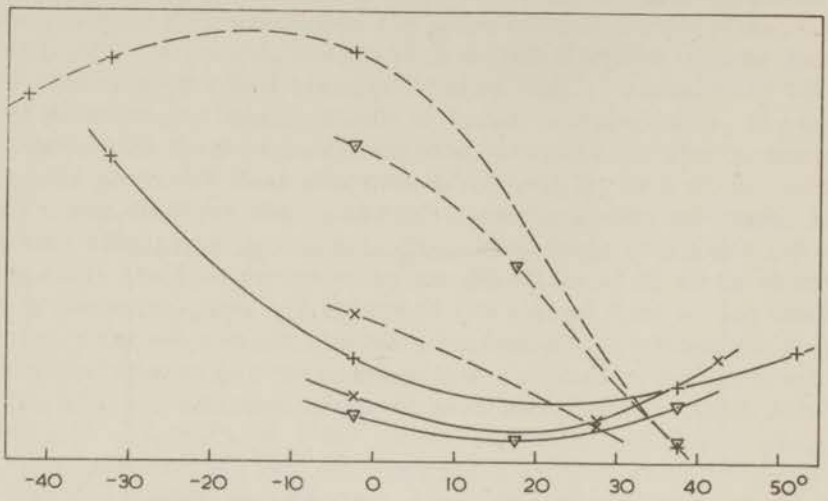

Fig. 11. Maximum absorptions versus θ in the 3 cm-a,c-case.
∇ T = 2.53_3°K ——— max. abs. at the lower resonance field
$\times$ T = 1.89_5°K - - - - max. abs. at the higher resonance field
$+$ T = 1.31_2°K

5. *Remarks.* The line widths did not reproduce very well. For **H** parallel to the *X*-axis, they were on the order of 100 Ø at the lowest temperatures, increasing with temperature slowly, at first, and then rapidly, at the higher temperatures. When **H** is rotated from the *X*-axis, the line widths generally increase. In a few cases the data are sufficient to show that this increase may roughly be explained by the fact that, in measuring, we are cutting through the absorption ridge in an oblique way.

In nearly all the measurements a peak was observed at the paramagnetic resonance field. We are inclined to describe this to some copper ions not fitting properly into the lattice of the antiferromagnetic crystal, thus giving rise to absorption by paramagnetic resonance. The following facts support this assumption:

a. In the a,b-crystal the paramagnetic peak was small but increased in the course of time. Apparently the crystal disintegrated slowly and more or less steadily.

b. In the measurements on the a,c-crystal, which had to be disqualified because of the bad condition of the sample (cf. introduction of this chapter), this effect was relatively large. It became more pronounced after further disintegration.

c. The intensity of absorption in this peak, as a function of the orientation of the field, shows the same character as the paramagnetic peak at hydrogen temperatures.

In the a,b-crystal, a small peak was observed several times just on the high field side of the second peak. Since it was a very small effect and since we dit not observe it in the a,c-case, we have not paid much attention to it.

The dispersion was measured qualitatively in a number of cases by observing the change in the resonant frequency of the cavity (cf.Ch.II,sec.3.4). In the neighbourhood of the paramagnetic peak and the higher field resonance peak along the X-axis, the dispersion showed a normal behaviour, that is, there was a dip on the low field side and a peak on the high field side of the absorption peak. In the neighbourhood of the lower field resonance peak, however, the behaviour was reversed. In the X,Y-case, when the external field was rotated from the X-axis, and the two absorption peaks coalesced, there was only a flat peak in the dispersion near the one remaining absorption peak.

C. The 7 cm antiferromagnetic resonance measurements

The 7 cm resonance measurements were carried out on the a,c-crystal. Thus, the external field **H** was confined to the X,Z-plane. In the first measurements on this crystal absorption lines were obtained whose properties may be described briefly as follows:

One line is obtained at low temperatures when **H** is directed parallel to the X-axis. Sometimes the presence of a second line is indicated by a distortion of the first line. The line moves up to higher field values when **H** is rotated towards the Z-axis. The evidence of the second line may become more pronounced.

At higher temperatures there are two maxima of absorption occurring on either side of the low temperature field value. We hardly can speak of lines as the shapes of the absorption curves are often rather peculiar. The maxima again move up to higher field values when **H** is rotated from the X-axis towards the Z-axis.

Thus, in the earlier 7 cm measurements, the properties of the „lines", i.e. their dependence upon temperature and on the orientation of the field, are qualitatively the same as at a wavelength of 3 cm.

In the later 7 cm experiments, however, an effect was observed, which seriously blurred this similarity. With increasing field, an absorption curve was obtained in which A increases, around a certain value H', varies slowly for $H \gtrsim H'$, and drops off to zero at a field value of about H''. When however, the field decreases from a value larger than H'', the absorption increases again, but around a value H''', of the field, considerably smaller

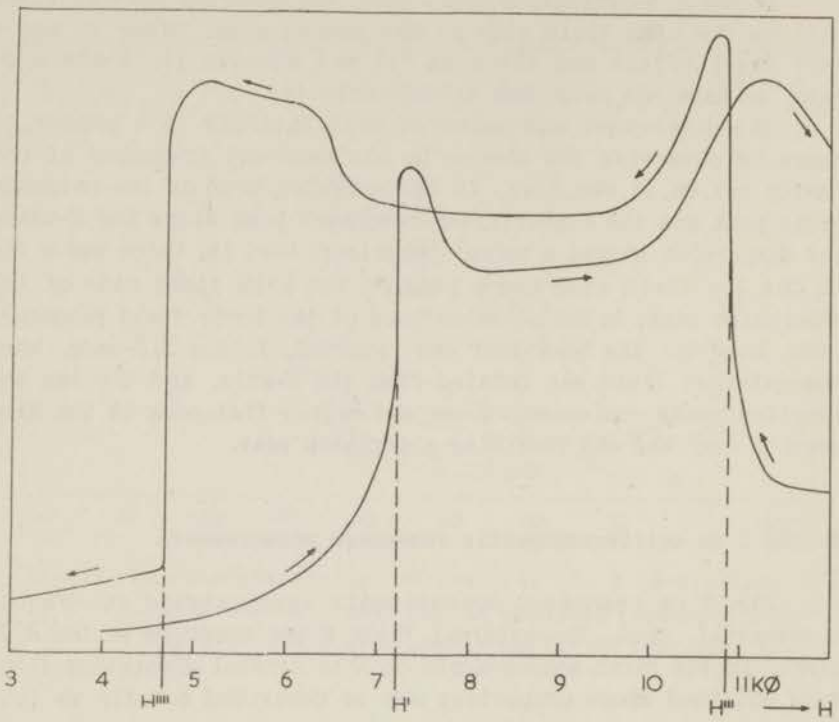

Fig.12. Absorption A versus magnetic field H at 7 cm, for increasing and decreasing field. $H \parallel a,c$-plane. Angle θ between **H** and a-axis = 33°. T = 3.72°K.

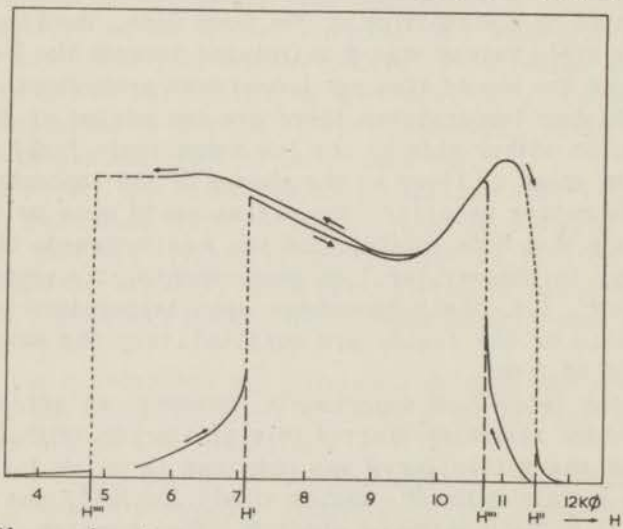

Fig.13. Absorption A versus magnetic field H at 7 cm, for increasing and decreasing field. $H \parallel a,c$-plane. Angle θ between **H** and a-axis = 33°. T = 3.72°K.

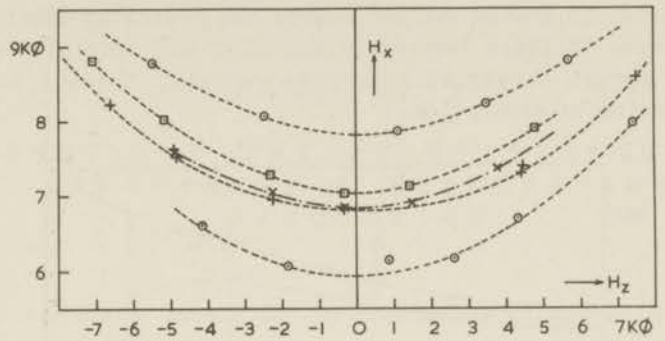

Fig.14. Line positions in the X,Z-plane, 7 cm.
⊙ T = 3.88°K. × T = 2.51°K.
⊡ T = 3.26°K. + T = 2.37°K.

than H'', and drops off again around a value H''', of the field, considerably smaller than H'. This effect may be described as quasi-hysteresis. Typical examples are shown in figures 12 and 13.

The effect shows several features which make it difficult to compile the results in diagrams like figures 5-7 for the 3 cm case. In the first place a marked maximum of absorption often is not observed. Then the change of absorption at the field values indicated above with $H' - H'''$, may be more or less gradual as well as very abrupt. The field values $H' - H'''$ are difficult to reproduce. Then a time effect was observed. When e.g. the field was increased quickly from zero to a field value somewhat larger than H', the absorption did not follow immediately, but increased slowly, becoming larger than the corresponding absorption obtained with slowly increasing field, and then reduced to this value, the whole process covering a period of the order of one minute. Another example is the case where H'', being too large, could not be observed. When the field was increased quickly to the largest value obtainable, practically zero absorption was observed, unlike the result with slowly increasing field. Then, when the field was decreased slowly, the absorption increased sharply at a certain value (H''') of the field.

Due to these complications it is not possible to give a complete survey of the results. We may state generally that the hysteresis becomes larger when either the temperature increases or the deviation of the field direction from the X-axis increases.

In fig.14 we give the results of the earlier measurements in which reasonable maxima of absorption were obtained. The X-axis is taken to be the axis with respect to which the results are symmetric to a reasonable degree.

In figures 15 and 16 we give the results for field directions along the X-axis and 33° out of the X-axis as functions of temperature. In these figures values of $H^{\prime} - H^{\prime\prime\prime\prime}$ are plotted only when an abrupt change of absorption occurs. Crosses indicate marked maxima of absorption.

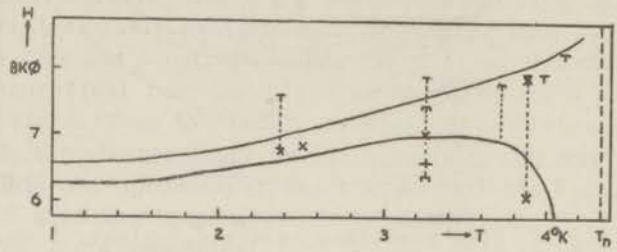

Fig.15. Fields at which abrupt changes of absorption occur versus temperature $\mathbf{H} \parallel a$-axis, 7 cm.

$\perp H^{\prime}$, $\top H^{\prime\prime}$, $\top H^{\prime\prime\prime}$, $\perp H^{\prime\prime\prime\prime}$.

× marked maximum absorption fields.

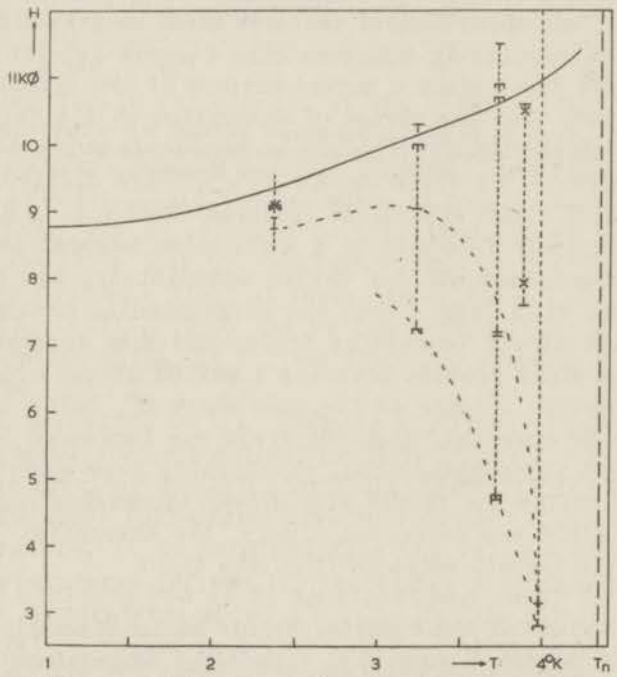

Fig.16. Fields at which abrupt changes of absorption occur versus temperature, 7 cm. $\mathbf{H} \parallel a,c$-plane. Angle between $\mathbf{H}$ and a-axis in 33°.

$\perp H^{\prime}$, $\top H^{\prime\prime}$, $\top H^{\prime\prime\prime}$, $\perp H^{\prime\prime\prime\prime}$.

× marked maximum absorption fields.

Chapter IV

THEORETICAL INTERPRETATION OF THE EXPERIMENTAL RESULTS AND DISCUSSION

1. *The resonance curves in the coordinate planes at 3 cm wavelength*

When we compare the experimental resonance curves in the coordinate planes as obtained at the lowest temperatures (Ch.III, figures 5 and 6) with the theoretical curves for $T = 0$, Ch.I, fig.5, stage 2, we see that they are in qualitative agreement. Apparantly only the tunneling part of the resonance surface has been observed. Therefore, we will apply the theory of Ch.I, sec. B.3 to the experiments, using the approximation in which terms of the order of h, a, b and c are neglected with respect to terms of the order of γ.

Fig.7 of Ch.III shows that the resonance fields along the X-axis are practically independent of temperature below $2^{\circ}K$. Therefore, we will assume that the resonance fields along the X-axis for $0^{\circ}K$ are given by the experimental ones at the lowest temperatures. The values of a, b and c are now obtained from the frequency and the resonance fields along the X-axis in the following way:

The higher resonance field is determined by formulae (29,30, 31) of Ch.I,B with $\Delta = 0$. With $h_z = 0$, we obtain

$$c^2 = h_x^2 - \varepsilon^2. \tag{1}$$

Introducing $H_c = c/\mu_x$, $H_2 = h_x/\mu_x$, $H_{px} = \varepsilon/\mu_x$ we obtain

$$H_c^2 = H_2^2 - H_{px}^2. \tag{2}$$

H_{px} is the field at which paramagnetic resonance occurs along the X-axis for the given frequency. From the 3 cm paramagnetic resonance measurements we have $H_{px} = 3.09$ KØ. H_2 is the higher antiferromagnetic resonance field along the X-axis and, from Ch.III fig.7, we have $H_2 = 7.25$ kØ. Introducing these values in (2), we obtain $H_c = 6.56$ kØ.

The lower resonance field is determined by formulae (32,33, 34) of Ch.I,B with $\Delta = 0$. With $h_z = 0$ we obtain:

$$\varepsilon^4 - (b^2 + c^2 + 2h_x^2)^2 + (b^2 - h_x^2)(c^2 - h_x^2) = 0. \qquad (3)$$

Introducing further $H_b = b/\mu_x$, we have

$$H_{px}^4 - (H_b^2 + H_c^2 + 2H_1^2)H_{px}^2 + (H_b^2 - H_1^2)(H_c^2 - H_1^2) = 0. \qquad (4)$$

From fig.7 Ch.III we would have for the lower resonance field $H_1 = 5.05$ kØ. Formula (4) then would yield $H_b = 12.54$ kØ and with $b^2 = a^2 + c^2$, we would obtain $H_a = a/\mu_x = 10.69$ kØ. Using these values of H_a and H_b we might calculate the theoretical resonance curves in the coordinate planes. A better fit with *all* the experimental points at the lowest temperatures in the X,Z-plane (Ch.III, fig.6), however, is obtained if we introduce a somewhat different value for H_b, namely $H_b = 11.71$ kØ, which yields $H_a = 9.71$ kØ. We have used these latter values in the following calculations.

The upper branch in Ch.III, fig.6 is obtained with

$$H_x^2/(H_c^2 + H_{px}^2) - \mu_z^2 H_z^2/\mu_x^2(H_a^2 - H_{px}^2) - 1 = 0, \qquad (5)$$

which, with the usual approximation, follows from Ch.I, sec.B.3, (29,30,31) with $\Delta = 0$. We took $\mu_z/\mu_x = g_c/g_a = 1.03$, following from the g-values as obtained by Ігон[27].

The lower branch involves somewhat more complicated calculations. From Ch.I,B.3,(32,33,34) with $\Delta = 0$ we have

$$Z^3 - Z^2(H'^2 + H_a^2 - H_c^2 + H_{px}^2) + ZH_{px}^2(-3H'^2 + H_a^2 - H_c^2 + 2H_{px}^2) - 2H_{px}^2(H_b^4 - H'^4) = 0 \qquad (6)$$

where $Z = z/\mu^2$ and $H' = h/\mu$.

Points of the lower branch (Ch.III, fig.6) are obtained by the following procedure:

1) give H' a series of values;
2) solve (6) for Z numerically for each of these values;
3) calculate θ from (cf.Ch.I, A.8, (57))

$$\cos 2\theta = (H^4 + H'^2 - Z^2)/2H_b^2 H'^2; \qquad (7)$$

4) calculate the coordinates of the points with

$$H_x = H' \cos\theta \qquad (8)$$

$$H_z = (\mu_x/\mu_z)H' \sin\theta \qquad (9)$$

The theoretical curve in Ch.III, fig.5 is obtained similarly, using a formula obtained from (6) by interchange of H_b^2 and H_c^2 and of H_a^2 and $-H_a^2$. In step 4 we have to take $H_y=(\mu_x/\mu_y)H'\sin\theta$, with $\mu_x/\mu_y = 1.06$ (cf.ref.27).

Because of the uncertainties in the calibration of the magnetic fields and the inaccuracy of the determination of the orientation of the crystal axes with respect to the apparatus, there does not seem to be much sense in applying the exact theory to the results, involving, as it would, much more complicated calculations.

As may be inferred from Ch.I, fig.5, stage 2, a small rotation of the plane, to which **h** is confined experimentally, from the coordinate plane with which it was supposed to coincide, will have a large effect – especially in the X,Z-case. A sufficient rotation of the experimental plane about the X-axis and away from the X,Z-plane will cause both branches to meet. The asymmetries still present in Ch.III, fig.6 may result from such rotations.

2. *The resonance fields along the axes as functions of temperature at 3 cm wavelength*

In the main, we shall confine the discussion to the resonance fields along the X-axis. According to YOSIDA there are two resonance fields, one for $H<H_c$ and one for $H<H_c$. The resonance condition for $H>H_c$ is given by Ch.I, B, eq.(20):

$$\{(\omega/\gamma)^2 - H^2 + 2AK_1\}\{(\omega/\gamma)^2 + 2AK_1 - 2AK_2\} = 0. \qquad (10)$$

Thus the upper resonance field $H_2>H_c$ is given by

$$H_2^2 = (\omega/\gamma)^2 + 2AK_1. \qquad (11)$$

Now, ω/γ is the field at which paramagnetic resonance occurs for a frequency ω and we write again $\omega/\gamma = H_{px}$. Further, $2AK_1 = \alpha H_c^2$ (cf.Ch.I, A, eq(26)) where H_c is the critical field at which the flop-over of spins occurs and is temperature dependent; for $T = 0$ it reduces to the H_c introduced in sec.1. According to the measurements of VAN DEN HANDEL et.al.[11], H_c increases slowly with increasing temperature.

Therefore, eq.(11) can be rewritten

$$H_2^2 = H_{px}^2 + \alpha H_c^2 \qquad (12)$$

Since, for temperatures greater than about half the Néel temperature, α decreases much more rapidly than H_c^2 increases with increasing temperature, the higher resonance field should decrease with increasing temperature. At a certain temperature T_1, however, H_2 and H_c will meet and, since H_2, determined by (12), is only a real resonance field for $H_2 > H_c$, the resonance line is „cut off" by the critical field at temperatures greater than T_1. Since the resonance line has a certain width, we still may observe the tail of the theoretical resonance line on the high field side of the critical field. Thus the theory predicts asymmetrical resonance lines with the steeper slope on the low field side when $T > T_1$, at $H \approx H_c$. This may account for the increase of the higher absorption field when the temperature increases (cf. Ch. III, fig. 7) and, partly, for the asymmetrical line shapes. This is an explanation already suggested by YOSIDA[22]. The „threshold absorption" (Ch. III, fig. 9), however, cannot be explained by it; but another interpretation offers itself in the form of the second factor of (10) which yields the resonance condition

$$H_{px}^2 = \alpha H_b^2 - \alpha H_c^2 = \alpha H_a^2 \quad \text{or} \quad \alpha = H_{px}^2 / H_a^2 \tag{13}$$

where we put $2AK_2 = \alpha H_b^2$.
This absorption is independent of the external field but only present for $H > H_c$; it should occur at a temperature T_2, defined by (13). It is very probable that the threshold absorption, observed at $T = 4.22^{\circ}K$ (cf. Ch. III, fig. 9), which is roughly field independent for $H > H_c$, may be ascribed to this theoretical absorption. Also, it is likely that the constant absorption for fields beyond the higher resonance field at lower temperatures ($T = 4.11^{\circ}K$ and $T = 3.98^{\circ}K$, Ch. III fig. 9) may be considered to be a „tail" of this absorption which, at a given frequency, depends only on the temperature.

Thus, according to the resonance condition (12), as well as (13), the upper absorption line, or at least its low field slope, yields the critical field H_c for $T > T_1$. In Ch. III fig. 7 we shall suppose the upper full-drawn curve to represent H_c as a function of temperature. It is obtained from the value 6.56 kØ at the lowest temperatures (cf. sec. 1), the higher resonance absorption fields at temperatures above $3^{\circ}K$ and a smooth interpolation in the temperature region in between. The point marked + in Ch. III fig. 7 represents the value of H_c obtained in the proton resonance measurements of POULIS et.al.[12] and is seen to agree well with our values of H_c. The assumed H_c values lie within the field regions where a steep increase of the susceptibility occurs according to the measurements of VAN DEN HANDEL et.al.[11].

According to the molecular field theory, any interaction between the two spin systems is proportional to S^2, the square of the average spin per sublattice. Thus the anisotropy constants K_1 and K_2 depend upon temperature in the same way as S^2, as was also shows by YOSIDA (cf. Ch. I, A. 4, eq. (21)). Therefore, we shall assume H_a, H_b and H_c to depend upon temperature in the same way and derive values of H_b and H_a from H_c by multiplying H_c with $H_b(0)/H_c(0)$ and $H_a(0)/H_c(0)$, taking the values of $H_a(0)$, $H_b(0)$ and $H_c(0)$ from sec. 1.

The quantity $\alpha = 1 - \chi_{\parallel}/\chi_{\perp}$ plays an important rôle in the discussion of the resonance fields. In YOSIDA's theory, the anisotropy of the g-value has been neglected. When this is taken into account it may be seen, by balancing the magnetic energy and the anisotropy energy, that in the formula for the critical field H_c,

$$\alpha H_c^2 = 2AK_1 \tag{14}$$

we have to take

$$A = 1/\chi_{ab} \tag{15}$$

and

$$\alpha = 1 - \chi_{aa}/\chi_{ab} \tag{16}$$

where the first subscript refers to the direction of the external field and the second to the direction of the spins. From GORTER and HAANTJES' theory it follows that

$$\chi_{ab} = (g_a^2/g_b^2)\chi_{ba}. \tag{17}$$

Thus we have also

$$\alpha = 1 - (g_b^2/g_a^2)\chi_{aa}/\chi_{ba}. \tag{18}$$

χ_{aa} corresponds to the condition $H \parallel X$-axis and $H<H_c$; χ_{ab} to $H \parallel X$-axis, $H>H_c$ and χ_{ab} to $H \parallel Y$-axis. When we introduce the values of these quantities, as obtained by VAN DEN HANDEL et. al.[11], into (16) and (18) we obtain α as a function of temperature (see fig. 1 curve 1).

From the H_c-curve of Ch. III fig. 7 and the α-curve of fig. 1, we obtain via (12) the upper resonance field H_2 as a function of temperature. This is shown by the dashed curve in Ch. III fig. 7. The temperature T_1 at which H_2 and H_c meet should be $T_1 = 2.3_5{}^{\circ}\mathrm{K}$. The experimental points do not show the dip in the curve of the higher absorption field, as a function of temperature, predicted by the curves for H_c and H_2. The experimental points in this

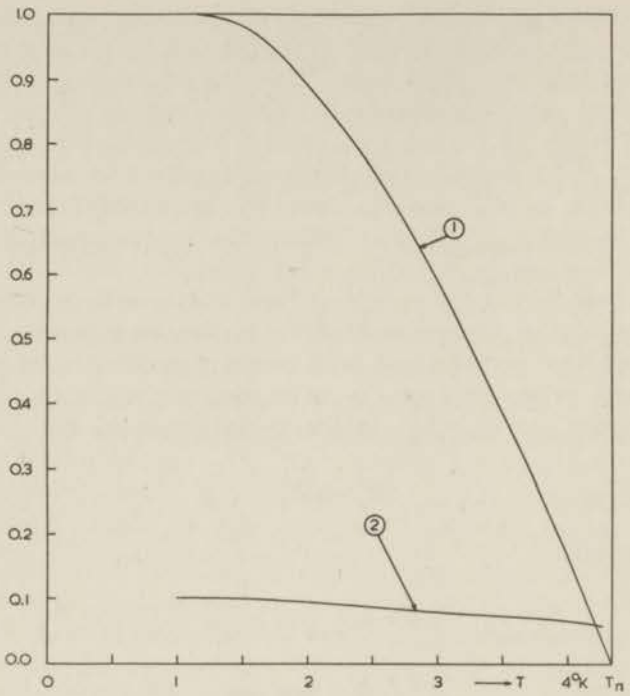

Fig. 1. curve 1: α versus T.
curve 2: H_{px}^2/H_a^2 versus T.

region, however, are too scarce to justify the statement that such a dip does not exist. The discrepancy between the curves and the experimental points at $T = 1.89$ and $T = 2.54^{\circ}$K might be diminished if the H_c-values are taken to be greater in this region. An increase of the H_c-values sufficient to remove the discrepancies, however, would involve an H_c-curve of a scarcely acceptable shape. Therefore, we will use the H_c-curve as drawn in Ch. III fig. 7, noting, however, that it is rather uncertain especially in the region around T_1.

When these adopted values for H_c and α are introduced into (14), K_1, as a function of temperature, is represented by curve 4 in Ch. I, A fig. 3. As mentioned before, it should depend upon temperature in the same way as S^2. It can be seen that there is a considerable discrepancy between curve 4 and the corresponding curve from the molecular field theory, as well as the curve from the experiments of POULIS.

The temperature T_2, at which the field-independent absorption above the critical field should occur, follows from (13). Curve 2 in fig. 1 represents H_{px}^2/H_a^2 (where $H_a = H_c H_a(0)/H_c(0)$). According to (13), T_2 is given by the intersection of curves 1

and 2 which yields $T_2 = 4.2^{\circ}K$. It is indeed near this temperature that the threshold absorption has been observed. An accurate estimiation of T_2, however, cannot be based on the result of these absorption experiments. For this, it would be necessary to determine the absorption at some field well above the critical field for a number of closely spaced temperatures.

The lower resonance field H_1 along the X-axis is, according to YOSIDA, determined by (cf. Ch. I, B eq. (19))

$$\alpha^2 H_1^4 - H_1^2\{(1+\alpha^2)H_{px}^2 \; \alpha^2(H_b^2+H_c^2)\} + (\alpha H_b^2 - H_{px}^2)(\alpha H_c^2 - H_{px}^2) \quad 0. \quad (21)$$

In (21), the larger root for H_1^2 is always greater than H_c^2, thus only the smaller root applies. The lower full-drawn curve of Ch. III fig. 7 represents H_1 as given by (21) when α, H_c, H_b and H_{px} are taken as obtained above. For $T = T_N$, we have $\alpha = 0$ and (21) would yield $H_1 = H_{px}$ if we suppose that H_c does not become infinite for $T = T_N$. As this latter assumption is dubious, however, the curves for H_c and H_1 have been dashed for temperatures near T_N. In connection with the expected behaviour of H_1 for temperatures near T_N when H_c remains finite, it may be noted that TROUNSON et. al.[28] have found resonance absorption at a field which gradually decreased from the paramagnetic resonance field when the temperature was decreased from the Néel point.

It can be seen that the theoretical curve agrees very well with the experimental results for temperatures below $4^{\circ}K$. A better fit at higher temperatures could hardly be expected here for the following reasons. First, because there are the discrepancies between the experimental points, which indicate imperfect thermal equilibrium in at least one of the series of measurements, and the great widths of the lines causing a large inaccuracy in the determination of the resonance fields. Second, the theory cannot be expected to give accurate results since the basic assumption of large exchange fields is no longer satisfied in this temperature region.

Resonance absorption with **H** *parallel to the Y-axis* might be expected when (cf. Ch. I, sec. B. 2)

$$(\omega/\gamma)^2 = H^2 + 2AK_1, \quad (22)$$

$$(\omega/\gamma)^2 = 2AK_2. \quad (23)$$

(23) corresponds to a field independent absorption at a particular temperature. It is difficult to detect since no variations

will be observed in the absorption versus H diagrams and the only was to establish the absorption is to compare absorptions at different temperatures, which is a delicate procedure.

Correcting (22) for anisotropic g-values, we obtain

$$H_{px}^2 = (g_b/g_a)^2 H_y^2 + \alpha H_c^2. \qquad (24)$$

Experimentally, resonance lines along the Y-axis are obtained at two temperatures, $T = 4.11^{\circ}$K and $T = 4.22^{\circ}$K (cf. Ch. III fig. 5). When we calculate α with these resonance fields, 1.20 and 2.25 kØ respectively, from (24) with $H_{px} = 3.09$ kØ, $g_a/g_b = 1.06$ and H_c from Ch. III fig. 7, we obtain the values 0.12 and 0.07, which agree well with curve 1 fig. 1.

Resonance lines along the Z-axis are not obtained experimentally.

3. *Discussion of the 7 cm results*

We have not been able to give a satisfactory interpretation of the hysteresis effect described in Ch. III, C. We suspect it to be a spurious effect, which has little to do with pure antiferromagnetic resonance.

Confining our attention, therefore, mainly to the cases where marked maxima of absorption were observed, we note in the first place that the curves of Ch. III fig. 14 show the same character as those of Ch. III. fig. 6. If the curves of both figures are assembled in one figure, the curves of fig. 14 will be found to arrange themselves neatly between those of fig. 6 for each temperature.

The fact that at the lowest temperatures (2.37; 2.51; 3.26°K) only one line is observed may be explained by the fact that the temperature T_1' at which the second resonance line H_2 and the critical cield H_c meet in the 7 cm case, is considerably lower than the former temperatures. An estimation of T_1' from (12), with $H_2 = H_c$, α and H_c from sec. 2 and $H_{px} = 1.28$ kØ, yields $T_1' = 1.6^{\circ}$K. Thus only H_1 will be observed.

Adopting this interpretation, formula (21) again relates α, H_c and H_1. The upper curve in III fig. 15 represents H_c, taken over from III fig. 7. The lower curve represents H_1 following from (21) with $H_{px} = 1.28$ kØ, the other quantities having the same values as before. A better agreement between the H_1-curve and the experimental points at the two lowest temperatures may be obtained by increasing the assumed values of H_c in this temperature region. Also, as seen before, the higher absorption fields at 3 cm point to larger H_c-values in this region, but these would involve

a scarcely acceptable curve of H_c versus T, and, moreover, they would spoil the agreement between the H_1-curve and the experimental H_1-values at 3 cm.

The critical field $H_c(\theta)$ in the X,Z-plane with an arbitrary direction which makes an angle θ with the X-axis, as a function of temperature, is obtained from Ch.I sec.A.9,(67). Correcting this equation for anisotropic g-values we have

$$H_x^2/H_c^2 - (g_c/g_a)^2 H_z^2/H_a^2 - 1 = 0, \qquad (25)$$

which yields

$$H_c(\theta) = H_c/\{\cos^2\theta - (g_c H_c/g_a H_a)^2 \sin^2\theta\}^{\frac{1}{2}} \qquad (26)$$

With $\theta = 33^\circ$, corresponding to Ch.III fig.16, $g_c/g_a = 1.03$, $H_c/H_a = H_c(0)/H_a(0)$ from sec.1, we obtain $H_c(33^\circ) = H_c/0.747$. Taking for H_c the upper full-drawn curve of III fig.7 we obtain for $H_c(33^\circ)$ the full-drawn curve in III fig.16.

Figures 15 and 16 of Ch.III suggest that the field values H'' and H''' at which the absorption decreases or increases sharply for, respectively, increasing or decreasing field, are related to the critical field. A close agreement between these fields and the critical field is not obtained however.

It seems probable that the field values at which the absorption increases (decreases) sharply for increasing (decreasing) fields are related to the lower resonance field. Why such a sharp change of absorption occurs, and why there is a hysteresis effect, remains obscure.

4. *Final remarks*

The qualitative measurements of the dispersion (cf.Ch.III, sec.B.5) are quite in agreement with theory. According to the KRAMERS – KRONIG relations (cf. e.g.ref.29), which relate the real part χ' of the susceptibility (dispersion) uniquely to the imaginary part χ'' (absorption) when the latter is known for any frequency, χ' as a function of frequency shows a peak just below and a dip just above the frequency at which a sharp peak of absorption occurs. When, now, the external field is changed and the frequency is kept constant, it will depend on the sign of $dH/d\nu$ of the resonance curve in the H,ν-plane if the dip comes before or after the peak in the dispersion curve when H increases. A glance at Ch.I fig.4 shows that the sign of $dH/d\nu$ for the lower

antiferromagnetic resonance field is opposite to that for the higher resonance field and the paramagnetic resonance field.

An interpretation of the polarization effect, i.e. the dependence of the intensity of absorption on the direction of the oscillating field (Ch.III, sec.B.4) has not yet been given. For this it will be necessary to study the equations for the first order time dependent parts of the magnetizations and of the magnetic field, which follow from the equations of motion for the magnetizations. Here, the time dependent part of the magnetic field will represent the oscillating field.

SAMENVATTING

Dit proefschrift heeft tot onderwerp de antiferromagnetische resonantie in koperchloride, $CuCl_2.2H_2O$, bij twee frequenties in het microgolvengebied.

In hoofdstuk I, deel A, wordt een overzicht gegeven van de moleculaire veld-theorie van het antiferromagnetisme in het algemeen zoals deze ontwikkeld is door NÉEL en anderen. Op basis van deze theorie wordt in deel B een theoretische analyse van de antiferromagnetische resonantie bij het absolute nulpunt gegeven en een overzicht van het werk van YOSIDA in dit gebied.

De methode die voor dit onderzoek van de antiferromagnetische resonantie absorptie gebruikt is, is de transmissie-absorptiemethode. Hierbij wordt de verzwakking in de stof van electromagnetische golven, die door een trilholte in resonantie worden doorgelaten, bepaald. Deze methode en de gebruikte opstelling worden in hoofdstuk II beschreven (zie II, fig.1).

De resultaten zijn in hoofdstuk III weergegeven. De belangrijkste hiervan betreffen de waarden der velden waarbij resonantie optreedt. Deze resultaten kunnen kort als volgt worden samengevat. Zet men de resonantievelden uit in de veldruimte, waarbij de X-, Y- en Z-as respectievelijk evenwijdig worden gekozen aan de a-, b- en c-as van het koperchloride-kristal, dan vindt men bij de laagste temperaturen ($\approx 1^{\circ}K$) in het X,Y-vlak een gesloten kromme om het punt op de X-as dat correspondeert met het critische veld waarbij de practisch antiparallele magnetisatierichtingen van de beide subroosters omklappen van de a-as naar de b-as. Deze gesloten kromme dijt uit wanneer de temperatuur toeneemt (III, fig. 5). In het X,Z-vlak vindt men, ter weerszijden van de critische hyperbool waarbij de spins omklappen, hyperbool-achtige krommen, die zich van elkaar verwijderen bij toenemende temperatuur (III, fig.6).

In hoofdstuk IV worden deze resultaten vergeleken met de theoretische beschouwingen uit hoofdstuk I. Het blijkt dat de moleculaire veld-theorie van het antiferromagnetisme in staat is deze resultaten zeer bevredigend qualitatief te verklaren. Er zijn echter enkele quantitatieve verschillen, welke nauw samenhangen met de afwijkingen van het magnetisch en calorisch gedrag van koperchloride van de moleculaire veld-theorie van het antiferromagnetisme.

REFERENCES

1. Gorter, C. J. and Haantjes, J., Commun. Kamerlingh Onnes Lab., Leiden, Suppl. 104b; Physica **18** (1952) 285.
2. Neel, L., Ann. Physique (10) **18** (1932) 5; (11) **5** (1936) 232; (12) **3** (1948) 137.
3. Bitter, F., Phys. Rev. **54** (1938) 79.
4. Van Vleck, J. H., J. chem. Phys. **9** (1941) 85.
5. Garrett, C. G. B., J. chem. Phys. **19** (1951) 1154.
6. Nagamiya, T., Prog. theor. Phys. **6** (1951) 342.
7. Yosida, K., Prog. theor. Phys. **6** (1951) 691.
8. Yosida, K., Prog. theor. Phys. **7** (1952) 25.
9. Van Vleck, J. H., Phys. Rev. **52** (1937) 1178.
10. Friedberg, S. A., Commun. 289d; Physica **18** (1952) 714.
11. Van den Handel, J., Gijsman, H. M., and Poulis, N. J., Commun. 290c; Physica **18** (1952) 862.
12. Poulis, N. J., and Hardeman, G. E. G., Commun. 287a and 288b; Physica **18** (1952) 201 and 315; another paper is to the press.
13. Anderson, P. W., Phys. Rev. **79** (1950) 705.
14. Yin-Yuan Li, Phys. Rev. **80** (1950) 457.
15. Yin-Yuan Li, Phys. Rev. **84** (1951) 721.
16. Weiss, P. R., Phys. Rev. **74** (1948) 1493.
17. Bethe, H. A., Proc. Roy. Soc. (London) **150A** (1935) 552.
18. Hulthen, L., Proc. Kon. Akad. v. Wetensch. Amsterdam **39** (1936) 190.
19. Anderson, P. W., Phys. Rev. **86** (1952) 694.
20. Kubo, R., Phys. Rev. **87** (1952) 568.
21. Nakamura, T., Prog. theor. Phys. **7** (1952) 539.
22. Yosida, K., Prog. theor. Phys. **7** (1952) 425.
23. Ubbink, J., Commun. Suppl. 105b; Physica **18** (1952).
24. Nagamiya, T., Prog. theor. Phys. **6** (1951) 350.
25. Keffer, F., and Kittel, C., Phys. Rev. **85** (1952) 329.
26. Bijl, D., thesis Leiden, 1950.
27. Itoh, J., Fujimoto, M., and Ibamoto, H., Phys. Rev. **83** (1951) 852.
28. Trounson, E. P., Bleil, D. F., Wangsness, R. K., and Maxwell, L. R., Phys. Rev. **79** (1950) 542.
29. Kronig, R., Ned. T. v. Nat., **9** (1942) 402.

STELLINGEN

I

De onderstelling van VAN VLECK in zijn theorie van het antiferromagnetisme dat de verschilvector van de gemiddelde spinvectoren van de twee subroosters scheef kan staan ten opzichte van het uitwendige veld is mathematisch in strijd met de vergelijkingen waarop de theorie gebouwd is.

J.H.van Vleck, J.Chem.Phys.**9**(1941)85.

II

De resonantie-absorptie die TROUNSON en anderen gevonden hebben beneden de Néeltemperatuur in een veld waarbij paramagnetische resonantie boven het Néelpunt optreedt is waarschijnlijk niet toe te schrijven aan echte antiferromagnetische resonantie, doch aan resonantie van magnetische ionen die niet op ordelijke wijze in het antiferromagnetische rooster gerangschikt zijn.

Trounson, Bleil, Wangsness en Maxwell, Phys.Rev.**79**(1950)542.

III

Vrije radicalen zullen zeer geschikt blijken te zijn om met behulp van de methode der adiabatische demagnetisatie temperaturen ver beneden $1^{\circ}K$ te bereiken.

IV

Het onderzoek van de matrixvergelijking $AB = \varepsilon BA$ kan op een eenvoudiger wijze worden uitgevoerd dan DRAZIN dit heeft gedaan.

M.P.Drazin, Proc.Cambridge Phil.Soc.**47**(1951)7.

V

Bij de beschouwing van de botsing van een interstellaire waterstofwolk met de schil van een nova is het niet juist te onderstellen dat de protonen, die door botsing ontstaan uit de waterstofatomen van de wolk, hoofdzakelijk geremd worden door scheiding van lading. De remming door ontmoeting met electronen uit de schil van de nova is belangrijker.

H.A.Kluyver, Proc. Symp. on the Motion of Gaseous Masses of Cosmical Dimensions, Paris, 1949, p.89.

VI

Bij de behandeling van de electromotorische kracht die opgewekt wordt in een draad, wentelend om de as van een permanente magneet, neemt ELIAS ten onrechte aan dat de electromotorische kracht opgewekt wordt in het gedeelte van de magneet dat met de draad een gesloten kromme vormt, en dat de electromotorische kracht in de draad verwaarloosd kan worden. Er wordt integendeel slechts in de draad een electromotorische kracht opgewekt.

G.J.Elias, Theorie van het electromagnetische veld (1948), II (2), p.194.

VII

De techniek der „micro-strips" biedt grote voordelen boven de thans gebruikelijke techniek in de radiospectroscopie bij lage temperaturen.

Proc.I.R.E., **40**(1952).

VIII

Hoewel ^{137}Cs verschillende voordelen boven ^{60}Co lijkt te hebben bij tele-therapeutisch gebruik, zal de grootte van de stralingsbron een ernstig bezwaar vormen, zelfs bij de grootst mogelijke concentratie van ^{137}Cs-kernen in deze bron.

IX

In het wiskundig criterium waaraan de zuiverheid van een evenredige stemming wordt afgemeten, dient aan de fout in de quint en in de grote terts een belangrijk groter gewicht te worden toegekend dan aan die in de harmonische zevende.

A.D.Fokker, Arch.Musée Teyler, **10**(1951)147.

X

Met een meter met wijzeraflezing waarbij een spiegel is aangebracht ter voorkoming van parallaxe kan een grotere nauwkeurigheid van aflezing verkregen worden door van de parallaxe van de naald ten opzichte van zijn spiegelbeeld gebruik te maken.

XI

Het is gewenst de keuze van onderwerpen bij het mathematisch onderwijs voor physische candidaten aan te passen aan de problemen die de physica stelt.

XII

Aan de voorgestelde bepaling dat pleziervaartuigen steeds zullen moeten wijken voor beroepsvaartuigen dient de consequentie verbonden te worden dat beroepsvaartuigen als zodanig door een duidelijk kenteken van pleziervaartuigen zijn te onderscheiden.